AD NUMBER
ADB004489
LIMITATION CHANGES

TO:

Approved for public release; distribution is unlimited.

FROM:

Distribution authorized to U.S. Gov't. agencies only; Test and Evaluation; APR 1975. Other requests shall be referred to Air Force Rome Air Development Center, IRRE, Griffiss AFB, NY 13441.

AUTHORITY

radc, usaf ltr, 27 Oct 1977

RADC-TR-75-119
Final Technical Report
April 1975

PARALLAX MEASUREMENT USING AN IMAGE MATCHED FILTER CORRELATOR

Harris Electronic Systems Division

D D C

JUN 13 1975

B

Rome Air Development Center
Air Force Systems Command
Griffiss Air Force Base, New York 13441

This report was prepared by the Electro-Optics Operation of Harris Electronic Systems Division, Melbourne, Florida, under Contract No. F30602-73-C-0312 with Rome Air Development Center, IRRE, Griffiss Air Force Base, Rome, New York. This effort was monitored by F. Scarano and J. Wasielewski of RADC/IRRE.

The Principal Investigator and Program Manager was F. B. Rotz, who reports to A. Vander Lugt, Director of Systems and Programs for the Electro-Optics Operation. Major contributors to this effort include M. W. Shareck, R. J. Straayer, and M. O. Greer; K. R. Porter provided assistance in the experimental effort.

Valuable support in the area of photogrammetry was provided by M. Geyer and G. Maupin of DBA, Inc. under a subcontract.

This report has been reviewed and approved for publication.

APPROVED:

JAMES E. WASIELEWSKI
Project Engineer

APPROVED:

HOWARD DAVIS
Technical Director
Intel & Recon Division

FOR THE COMMANDER:

JOHN P. HUSS
Acting Chief, Plans Office

Do not return this copy. Retain or destroy.

REPORT DOCUMENTATION PAGE		READ INSTRUCTIONS BEFORE COMPLETING FORM
1. REPORT NUMBER RADC-TR-75-119	2. GOVT ACCESSION NO.	3. RECIPIENT'S CATALOG NUMBER
4. TITLE (and Subtitle) PARALLAX MEASUREMENT USING AN IMAGE MATCHED FILTER CORRELATOR		5. TYPE OF REPORT & PERIOD COVERED Final Technical Report June 1973 – January 1975
		6. PERFORMING ORG. REPORT NUMBER N/A
7. AUTHOR(s) F. Rotz et al		8. CONTRACT OR GRANT NUMBER(s) F30602-73-C-0312
9. PERFORMING ORGANIZATION NAME AND ADDRESS Harris Electronic Systems Electro-Optics Operation Melbourne FL 32901		10. PROGRAM ELEMENT, PROJECT, TASK AREA & WORK UNIT NUMBERS 55690131
11. CONTROLLING OFFICE NAME AND ADDRESS Rome Air Development Center (IRRE) Griffiss AFB NY 13441		12. REPORT DATE April 1975
		13. NUMBER OF PAGES 93
14. MONITORING AGENCY NAME & ADDRESS(if different from Controlling Office) Same		15. SECURITY CLASS. (of this report) UNCLASSIFIED
		15a. DECLASSIFICATION/DOWNGRADING SCHEDULE N/A

16. DISTRIBUTION STATEMENT (of this Report)

Distribution limited to U. S. Gov't agencies only; test and evaluation; April 1975. Other requests for this document must be referred to RADC (IRRE) Griffiss AFB NY 13441.

17. DISTRIBUTION STATEMENT (of the abstract entered in Block 20, if different from Report)

Same

18. SUPPLEMENTARY NOTES

RADC Project Engineer:
JAMES E. WASIELEWSKI (IRRE)
AC 315 330-2621

19. KEY WORDS (Continue on reverse side if necessary and identify by block number)

Matched Filtering
Coherent Optics
Cartography

20. ABSTRACT (Continue on reverse side if necessary and identify by block number)

A breadboard coherent optical mapping system was tested and used to obtain parallax data in stereo aerial photographs. The system's performance was greatly improved by various modifications and by interfacing it to a mini-computer. Parallax data obtained from the system showed excellent agreement with similar data generated on an operational automatic stereocompilation system.

The coherent optical technique offers a number of unique advantages and, in

DD FORM 1 JAN 73 1473 EDITION OF 1 NOV 65 IS OBSOLETE

view of the breadboard system's good performance, recommendations for further development of this approach are given.

TABLE OF CONTENTS

TABLE OF CONTENTS
(continued)

LIST OF ILLUSTRATIONS

Evaluation

The value of this study to the Air Force's mission is that it examines the capability of a coherent optical data processing system which may increase the overall effectiveness of the mapping and cartographic operation. It has been demonstrated by this effort that a coherent optical parallax extraction system is comparable in performance to a digital stereoscopic extraction system. In fact, the optical system has certain advantages such as speed, accuracy, and self-correlation, which potentially make it superior to conventional digital parallax extraction systems. However, areas such as scanner location control and detector readout still require significant improvement before the optical system can attain its potential in an operational environment.

JAMES E. WASIELEWSKI
Project Engineer
Recon Info Systems Section
Recon & Mapping Branch

SECTION I

INTRODUCTION

SECTION I

INTRODUCTION

The objectives of the activities reported in this Final Report were to conduct experimental tests and to evaluate a large aperture frequency plane correlator which derives terrain elevation data from stereo aerial photography. Under Contract Number F30602-73-C-0312 with Rome Air Development Center, the Electronic Systems Division of Harris Corporation has performed a series of coherent optical correlation experiments with a breadboard system supplied by RADC.

During the course of these experiments, the equipment supplied by RADC was evaluated and modified to provide a higher level of system automation and improved system performance.

Experimental results from this effort demonstrate that parallax data obtained with the coherent optical correlator compares favorably with results from an operational electronic correlation system, the AS-11B. Quantitative comparisons have yielded an r.m.s. difference of less than 30μ along a profile, which is remarkably good in view of the limited sophistication of the present optical processing system. This report describes the experimental effort and results obtained in this study, and presents conclusions and recommendations.

Some background of automatic stereo compilation and the potential advantages of coherent optical techniques are covered in Section 1. Experimental results and their significance are summarized in Section 2, which also presents our conclusions and recommendations. Section 3 briefly covers the basic principles of coherent optical correlation and Section 4 describes the Image Matched Filter (COMAP) System, various modifications made to the system and alignment procedures. Experimental techniques including filter optimization input preprocessing and data collection are presented in

2

Section 5.   Calibration and data collection are covered in Section 6.   Data reduction and a comparison of COMAP and AS-11B parallax measurements. are found in Section 7.   The potential performance and advantages of a COMAP type system are discussed in Section 8.

SECTION II

SUMMARY AND CONCLUSIONS

SECTION II

SUMMARY AND CONCLUSIONS

In this section, we briefly discuss important characteristics of a COMAP system, summarize our experimental results, and present our conclusions and recommendations. Relevant supporting material is found in subsequent sections of this report; in particular, Section 7, which presents direct comparison of a COMAP and AS-11B parallax measurements.

2.1 AUTOMATIC STEREOCOMPILATION

Parallax differences in stereoscopic aerial photographs are used to determine ground elevation. Originally, manual stereoplotters or stereocomparitors were used to measure parallax in stereo photographs and produce contour lines or profile data. This method of stereocompilation is slow and requires the availability of highly skilled personnel and relatively precise and expensive equipment. Over the past two decades, several automatic stereocompilation systems have been developed. For the most part, these systems are based on scanning the aerial photos with a small spot and electronically cross-correlating the resulting video signals. Whereas these electronic correlation systems have been increasingly successful, there still exists room for improvement in various operational characteristics and cost. Therefore, it is desirable to explore alternative approaches to automatic stereocompilation which may avoid some limitations associated with electronic correlation schemes. In particular, coherent optical data processing (ODP) is an attractive method for automatic parallax measurement and it offers some unique advantages.

An automatic stereocompiler based on ODP can offer speed and accuracy equal to or surpassing electronic correlators. Most importantly, a coherent optical mapping (COMAP) system can automatically reacquire

5

correlation after passing through a region which will not produce useful correlation (e. g. a snow field or lake with no detail). Omni-directional air base capability is inherent and the air base need not be aligned with any particular axis in the system. Formatting of data points (x, y locations) is flexible, and the system may provide parallax data directly on a regular grid in model coordinates; this minimizes subsequent data reduction. A COMAP system can readily be designed to use the full resolution of imagery. It does not need sophisticated moving film platens and can be scaled to match various frame size requirements without significant loss in capability or accuracy. Whereas the cost of a fully operational COMAP system has not been firmly established, it should be cost competitive with systems based on electronic cross correlation. In particular, a field transportable, small format system could be accurate, rugged and relatively inexpensive.

The basis of the above-mentioned advantages of a COMAP system are discussed in other portions of this report.

2.2 EXPERIMENTAL RESULTS

The COMAP system was used to obtain parallax data along several scan lines in vertical frame, stereo photography of the Canadian Photogrammetric Test Range. The stereo pair used here contained a large number of surveyed control points and had previously been processed on the AS-11B automatic stereocompilation system.

A typical COMAP scan consisted of obtaining parallax readings at approximately two hundred points 0. 5 mm apart and in a direction orthogonal to the air base. Pertinent AS-11B data was used to calculate parallax along the nearest AS-11B scan line for comparison purposes. Parallax and position data for various control points were used to adjust the COMAP data to the AS-11B model system. Comparison of the COMAP and AS-11B parallaxes showed good agreement between them. The fit between COMAP and AS-11B data improved as more experience was gained

on the COMAP system. The final two data runs showed r.m.s. differences of 24μ and 30μ (model coordinates) between COMAP and AS-11B parallaxes when rotational and translational biases were removed. This is remarkably good agreement, especially in view of the fact that the COMAP and AS-11B scans were not exactly coincident and the AS-11B data itself contained an uncertainty of approximately 10μ. Moreover, the relatively unsophisticated instrumentation of the COMAP system undoubtedly yielded less accuracy than the system is actually capable of producing.

Details of the reduction and evaluation of the COMAP parallax data are presented in Section 7 of this report, where several examples of COMAP and AS-11B parallax profiles are given.

2.3   CONCLUSIONS

The basic feasibility of using coherent optical techniques for automatic stereo compilation has been demonstrated in this study. Analytical arguments indicate that a COMAP type system should be at least as accurate as one based on electronic correlation; this is supported by the good agreement between COMAP and AS-11B data. The potential speed of a coherent COMAP system should also equal or better that of a system requiring physical motion of the input photographs. The primary limitation on the speed of an optical correlator appears to be that imposed by the output detector and development of an adequate detection system could lead to a very high speed system (over $100 \text{ mm}^2/\text{sec}$ coverage).

One of the most important advantages of a COMAP system is that it will not get "lost" as a result of abrupt changes in parallax or in regions of poor correlation caused by lack of image detail. This results from the fact that the system cross correlates a small region with an entire frame rather than with another small region. This avoids the image overlap or lock-in problem associated with image-to-image correlators such as the AS-11.

The ability to avoid getting lost should allow a COMAP system to maintain a high average throughput rate and can minimize or eliminate the need for human intervention during parallax data collection.

A COMAP system has the interesting property that it can readily be scaled in size without appreciably affecting the accuracy of parallax measurements. Consequently, it is possible to conceive of a small, field-size version of a COMAP system designed for tactical use at a forward reconnaissance base.

2.4   RECOMMENDATIONS

The positive experimental results to date and the potential of the COMAP concept in terms of cost, speed, and operational flexibility justify further development of this system. The present breadboard system should be more fully instrumented and brought up to a quasi-operational status. The degree of automation added to the breadboard should be such that it is possible to gather large amounts of parallax data in a timely manner. Then the system can be used to generate a number of photogrammetric models using different types of imagery (vertical frame, convergent pan, etc.). This will provide a firm basis for estimating the actual performance which can be expected from an operational COMAP system.

SECTION III

PRINCIPLES OF COHERENT OPTICAL CROSS CORRELATION

SECTION III

PRINCIPLES OF COHERENT OPTICAL CROSS CORRELATION

Coherent optics has a natural application to the processing of two-dimensional imagery. Most significantly, optical processing allows parallel cross correlation of large quantities of data at high speeds. Sequential frame aerial photography is ideally suited to the input requirements of an optical processor.

Automatic techniques for extracting prallax information from a stereo pair typically involves cross correlating a small portion of one transparency with a second transparency. The position of the resulting cross correlation peak gives a direct measure of the resultant parallax in photo coordinates. In this section we will discuss the basic principles of using a coherent optical system to perform cross correlation.

3.1 GENERAL

The cross-correlation operation gives the best linear estimate of the similarity between two function. Stated mathematically, the cross-correlation between $f(x, y)$ and $h(x, y)$ is

$$r(u, v) = \int\int\limits_{-\infty}^{\infty} f(x, y) \, h(u+x, \ v+y) \, dxdy \tag{1}$$

Although the integrals in (1) are over infinite limits, it is understood that $f(x, y)$ and $h(x, y)$ are of finite extent.

The correlation function $r(u, v)$ is a measure of the degree of similarity between $f(x, y)$ and $h(x, y)$ as a function of the displacement variables (u, v). If the reference function $h(x, y)$ is contained in the frame $f(x, y)$, $r(u, v)$ will be a maximum at a specific set of values for u and v; these values can then be used to locate $h(x, y)$ relative to $f(x, y)$.
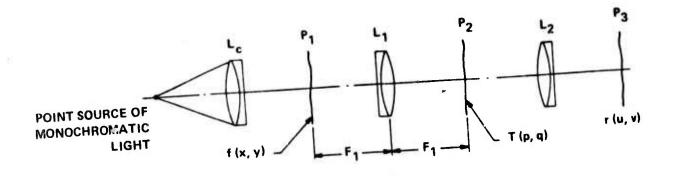
10

The correlation procedure requires, therefore, that $r(u, v)$ be calculated for each value of u and v, and that the location of the maximum value of $r(u, v)$ be located.

Aerial photographs contain a tremendous amount of information, typically over 10^8 bits per frame. This amount of information is easily handled by an optical system but represents a significant problem for digital techniques. Since the optical system is an analog device, quantizing and digitizing errors are not encountered in the calculation of $r(u, v)$. It is a parallel processor and is ideally suited for correlation of two-dimensional photography because of its inherent two-dimensional, nonscanning nature.

3.2   COHERENT OPTICAL SYSTEMS

Both incoherent and coherently illuminated optical systems have been used to evaluate the correlation function $r(u, v)$ as given in (1). The arrival of CW gas lasers as powerful and economical sources of spatially and temporarily coherent light make coherently illuminated systems practical and the clear choice over incoherently illuminated systems. Their superiority arises from their ability to display the Fourier transform of a two-dimensional input function so that the transform can be modified by a spatial filter and the corresponding filtering operation effected simultaneously over the entire input function.

Figure 3-1a shows the basic elements of a coherent optical data processing system. In describing the operation of the system we shall assume that photographic transparencies are used to input the data and for recording filters. A point source of monochromatic light, collimated by lens L_c, illuminates $f(x, y)$ which represents the data to be processed. A spherical lens L_1 displays the two-dimensional Fourier transform $F(p, q)$ of $f(x, y)$ at its back focal plane P_2. Although the Fourier transform relationship exists for a wide range of axial positions of $f(x, y)$, the

11

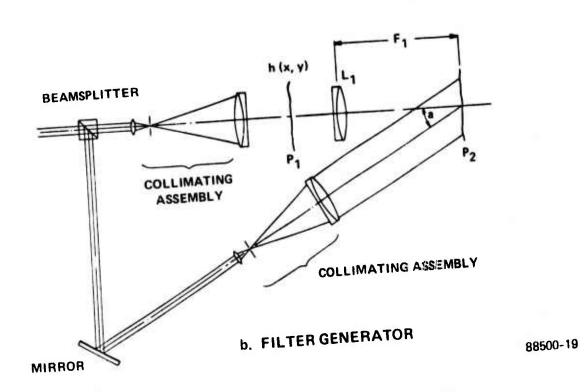a. BASIC ODP SYSTEM

b. FILTER GENERATOR

88500-19

FIGURE 3-1. BASIC ODP AND FILTER MAKING SYSTEM

optimum position of $f(x, y)$ is at the front focal plane of L_1. A spatial filter having transmittance $T(p, q)$ can be placed in plane P_2 to modify $F(p, q)$ directly. The amplitude $r(u, v)$ of the light in the output plane of the optical system is the Fourier transform of the wavefront emerging from the filter, i.e.,

$$r(u, v) \quad \frac{1}{4\pi^2} \iint_\Lambda F(p, q) \, T(p, q) \, e^{-j(px+qy)} \, dpdg. \tag{2}$$

The spatial frequency variables p and q are related to the space coordinates (ξ, η) in the plane P_2 by the relationships

$$p = \frac{2\pi\xi}{\lambda F_1} \,, \quad q = \frac{2\pi\eta}{\lambda F_1} \tag{3}$$

where λ is the wavelength of the illumination and F_1 is the focal length of L_1. If we apply the convolution theorem to the cross-correlation Eq. (1), we find that

$$r(u, v) = \frac{1}{4\pi^2} \int\int_{-\infty}^{\infty} f(x, y) \, t(u-x, \ v-y) \, dxdy, \tag{4}$$

and, if $t(x, y) = h(-x, -y)$, Eqs. (4) and (1) are identical. Equation (2) shows that the appropriate filter function $T(p, q)$ to be placed in plane P_2 is the conjugate of the Fourier transform of the reference function; i.e., $H^*(p, q)$. The cross-correlation function $r(u, v)$ is then formed by a second Fourier transform; lens L_2 is used for this purpose.

The required filter function $H^*(p, q)$ can be constructed as a spatial carrier-frequency filter. Figure 3-1b shows a filter-generator in which $h(x, y)$ is placed in plane P_1 and illuminated by a plane wave of monochromatic light. Lens L_1 displays the Fourier transform $H(p, q)$ at its back focal plane. A reference beam of light, denoted by $A \exp[jpb]$, is added to $H(p, q)$ and the intensity of the sum of these two light beams is recorded

13

on a high resolution photographic film or other suitable recording medium (e. g., a plastic device). The light intensity at plane P_2 is

$$|G(p, q)|^2 \quad |Ae^{jpb} + H(p, q)|^2$$

$$A^2 + |H(p, q)|^2 + Ae^{-jpb} H(p, q) + Ae^{jpb} H^*(p, q), \quad (5)$$

where $b = F_1 \tan \alpha$.

Because a coherently illuminated optical system is linear in light amplitude, we want to relate the amplitude transmittance of the recorded filter to the incident exposure. We characterize the linear portion of the amplitude transmittance versus exposure curve of a film by

$$T_a = T_o - \beta E, \quad (6)$$

where T_o is the amplitude intercept and β is the slope of the straight line. By substituting (5) into (6), we have

$$T_a(p, q) = \left[-\beta t \ (A^2 - T_o/\beta t) + |H(p, q)|^2 \right.$$

$$\left. + Ae^{-jpb} H(p, q) + Ae^{jpb} H^*(p, q) \right]. \quad (7)$$

Note that the last term of (7) contains the desired filter function $H^*(p, q)$; it remains to be shown that this term can be separated from the others.

After exposure and development, the filter $T_a(p, q)$ is placed in plane P_2 of the optical system shown in Figure 3-1a and is illuminated by $F(p, q)$. At the output plane P_3 of the processor, we observe three filtered versions of the input data:

14

$$r_1(-u, -v) = \frac{1}{4\pi^2} \int\limits_{-\infty}^{\infty}\!\!\int F(p, q)[(A^2 - T_0\beta t) + |H(p, q)|^2]e^{-j(pu+qv)} \, dpdq$$

$$r_2(-u, -v) \quad \frac{A}{4\pi^2} \int\limits_{-\infty}^{\infty}\!\!\int F(p, q) \, H(p, q)e^{-j[p(u-b) + qv]} \, dpdq$$

$$r_3(-u, -v) \quad \frac{A}{4\pi^2} \int\limits_{-\infty}^{\infty}\!\!\int F(p, q) \, H^*(p, q) \, e^{-j[p(u+b) + qv]} \, dpdq. \tag{8}$$

The first term of (8), centered on the optical axis, is generally of no interest.
The second term, centered at $u = -b$, represents the convolution of
$f(x, y)$ with $h(x, y)$. The third term, centered at $u = +b$, represents the
desired cross-correlation of $(\quad, y)$ and $h(x, y)$. If we bear in mind that
$r_3(-u, -v)$ is centered at $+b$, we may rewrite the third term as

$$r_3(-u, -v) = \frac{A}{4\pi^2} \int\limits_{-\infty}^{\infty}\!\!\int F(p, q) \, H^*(p, q)e^{-j(pu+qy)} \, dpdq, \tag{9}$$

which, through the use of the convolution theorem, is identical to (1).
The coordinates (u, v) in plane P_3 have reversed signs as a consequence
of the fact that a positive spherical lens always introduces a negative kernal
function in the Fourier transform operation. The negative coordinates imply
that the filtered image is rotated through 180 degrees, a natural result ob-
tained from any imaging system whether coherently or incoherently il-
luminated.

3.3   PARALLAX MEASUREMENT

A coherent optical correlator is used to determine parallax by
cross-correlating small regions in a stereo pair of transparencies. Let us
assume that one transparency $h(x, y)$ from a stereo pair is used to make a

spatial filter as described above. The second transparency, $f(x, y)$ and this filter are located in planes P_1 and P_2 respectively of the system shown in Figure 3-1a.

If only a small area of the second transparency is illuminated, the output plane P_3 will contain a light intensity pattern corresponding to the cross correlation of this illuminated area with that of the entire first transparency. Ideally, any given small area (A_h) will cross correlate strongly with only the corresponding small area (A_f) on the first transparency. The position of the cross correlation peak in plane P_3 is fixed by the relative positions of these two small areas $(A_h$ and $A_f)$ in the input gate. Any change in position for this region between the filter making operation and the cross correlation operation will cause a corresponding displacement shift of the correlation peak in the output plane. This correlation position shift can be used to measure the parallax between the local regions.

By sequentially illuminating portions of the second transparency, $f(x, y)$, and detecting the positions of the corresponding correlation peaks, we can measure parallax over the entire input scene.

16

SECTION IV

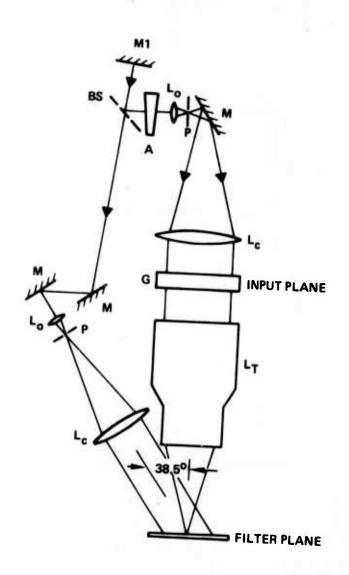# COMAP SYSTEM

SECTION IV

COMAP SYSTEM

A major task in this study was the evaluation and modification of
the breadboard Image Matched Filter System (COMAP) provided by
RADC. This section of the report describes the system and some of the
more significant modifications performed by us. While we were able to
considerably improve the performance of the system and obtain good
parallax data, some further modifications are desirable. Techniques used
in aligning and calibrating the system are also described in this section.

4.1 GENERAL CONFIGURATION

During this study, the COMAP system went through a series of
evolutionary changes involving the modification or relocation of some of
the original components as well as the addition of some of our in-house
equipment. However, the general configuration and function of the system
did not change substantially and only the final system arrangement will be
described in detail. A minicomputer was interfaced to the COMAP system
to aid in data collection.

The COMAP system used in this study operates in two different
modes: the filter generation mode or the data collection mode. The experi-
mental set up of the system is shown in the line diagrams of Figures 4-1
through 4-3. Figure 4-1 shows the configuration for filter generation,
while Figure 4-2 shows the system layout for the data collection mode.
Figure 4-3 schematically illustrates the minicomputer interface.

The COMAP processor was set up on a pneumatically supported
table. The components necessary for both modes of operation are present
simultaneously on the table, and the interchange between modes is easily
accomplished by repositioning only two mirrors: the beam routing mirror

18

M1 – BEAM ROUTING MIRROR   M   – MIRROR
BS – BEAM SPLITTER   G   – LIQUID GATE
A   – ADJUSTABLE ATTENUATOR   L_c – COLLIMATING LENS
L_o – MICROSCOPE OBJECTIVE   P   – PINHOLE
     L_T – FOURIER TRANSFORM LENS
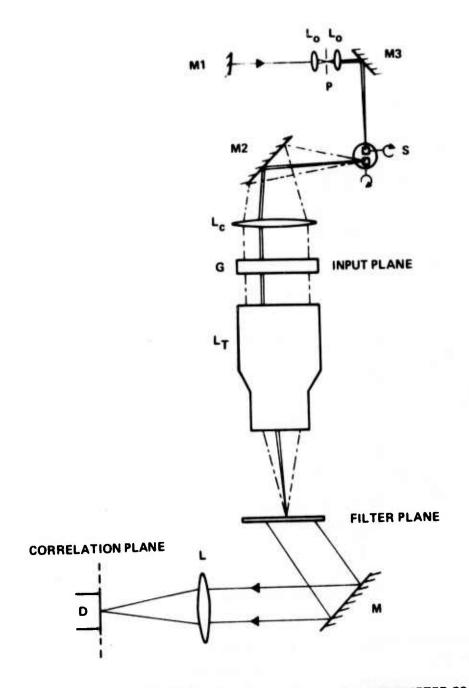
88500-1

FIGURE 4-1.   COMAP SYSTEM: FILTER GENERATION MODE

19

M1 — BEAM ROUTING MIRROR
L₀ — MICROSCOPE OBJECTIVE

S   — GALVONOMETER SCANNING UNIT
M2 — SCANNING MODE MIRROR
Lc — COLLIMATING LENS
G   — LIQUID GATE
L   — CORRELATION LENS
D   — CORRELATION DETECTOR

P   — PINHOLE
M   — MIRROR
LT — FOURIER TRANSFORM LENS

88500-2

FIGURE 4-2. COMAP SYSTEM: PARALLAX MEASUREMENT MODE

FIGURE 4-3.   COMAP SYSTEM: COMPUTER AND OPERATOR INTERFACE

21

M_1 and the scanning mode mirror M_2. A lens-pinhole assembly determines the correct orientation of M_1, and fixed stops locate M_2.
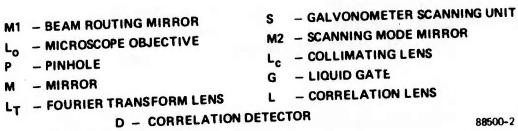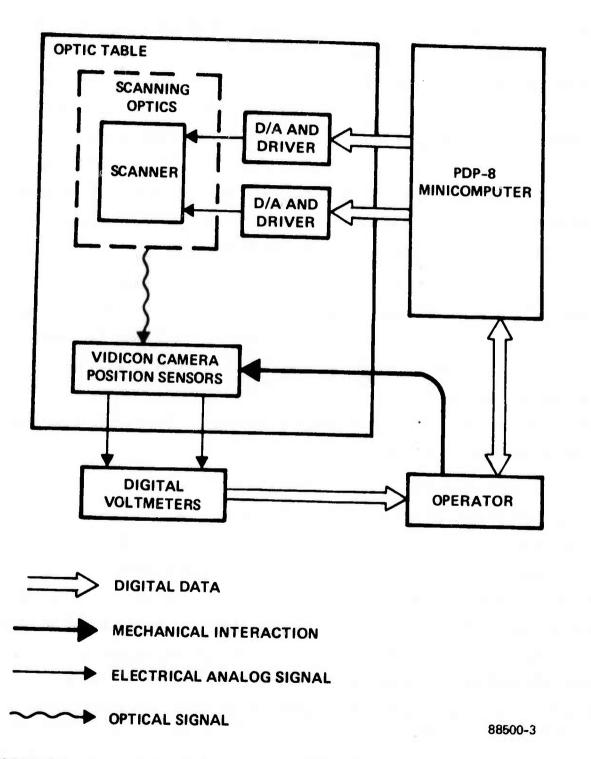
In the filter generation mode (Figure 4-1), the 514.5 nm light from a Spectra Physics 165 Argon ion laser is directed into the system by beam routing mirror M_1. The incident laser beam is split into a signal and a reference beam by a beamsplitter. The reference beam is then spatially filtered and collimated with its axis at an angle of 38.5° to the signal beam axis. The signal beam is also expanded and filtered by a lens-pinhole assembly and collimated by lens L_C. This collimated light is incident on the liquid gate G which contains a transparency (aerial photograph) for which a matched filter is to be produced. The lens L_T forms the Fourier transform of the input transparency in the filter plane. The axes of the reference and signal beams intersect at the filter plane.

The optical system arrangement for data collection is shown in Figure 4-2. The beam routing mirror M_1 is reoriented so that all of the laser light is directed to a telecentric galvanometer scanner. The beam in this case is formed in a narrow cone which illuminates an area approximately 1 mm in diameter in the input gate. The scanning beam routing mirror M_2 is translated into position against fixed stops when converting to the data collection mode.

The telecentric scanner consists of two small galvanometers with axes at right angles and whose mirrors are in the conjugate planes of a folded telescope. The scanner is positioned so that the scanning beam pinhole is imaged onto the center of both mirrors. This assures that the scanning beam always appears to come from the same point regardless of the direction in which it is deflected. The scanner and scanning beam optics are arranged so that the scanning beam is collimated at the input gate. Hence, the scanning beam pinhole is optically at the same position with respect to L_C as is the signal beam pinhole in the filter generation mode; i.e., one focal length away.

22

The Fourier transform lens L_T and the collimator L_C form a telescope which images the scanning beam source in the filter plane. When the system is properly aligned, this image of the scanning beam source is stationary regardless of the position the scanning beam in the input gate.

The spatial filter, when illuminated by a wavefront derived from a matched area from the input transparency, reconstructs a modified version of the original reference beam at a nominal angle of 38.5° to the optical axis. This beam is reflected by the mirror to the lens L which forms the cross correlations in the output (correlation) plane. This lens and mirror are mounted on a small auxiliary optical rail attached to the optical table.

A vidicon camera mounted on an X-Y translation device is used for measuring the locations of correlation peaks. Parallax measurements are made by translating the vidicon until the correlation peak, as viewed on a TV monitor, is centered on a pair of electronic cross hairs. A precision linear potentiometer on each axis of the camera translation device is connected to a digital multimeter arranged to measure resistance in a ratio mode. The least count on the digital meter corresponds to a translation of $1.5 \mu m$.

The scanner's galvanometers are interfaced to a minicomputer by means of two 12-bit D/A converters. We developed software to provide correction for the non-linear nature of the galvanometer scanner which allowed the operator to simply type in the photocoordinates of any desired point. The computer also provided a convenient and rapid means for stepping along a given scan line, or sequentially addressing a series of control points.

4.2   SYSTEM MODIFICATIONS

The final configuration of the COMAP system as described above came about after a series of modifications to the original equipment.

These modifications represented a considerable portion of the effort expended in this study and resulted in improved system performance.

We found, upon assembly of the COMAP system, that although the overall construction of the optical system appeared good, there were several problem areas which limited the performance of the system. These areas included stability of the optical bench, thermal effects in the liquid gate, and the correlation detection optics. These problems were corrected and the optical system was modified wherever necessary. Each problem is discussed briefly in this section.

The first step necessary to obtain good spatial filters is to establish a stable optical bench. This is particularly true for the high offset angle of the COMAP system. We found it was necessary to bolt each component firmly to the table and ensure that the supporting table legs were correctly aligned. It was also necessary to isolate the laser by installing rubber pads under it and by suspending the umbilical cord in order to eliminate vibrations caused by the flow of cooling water. The original system included a small cantilevered table extension which supported the reference beam turning mirror. This assembly tended to vibrate and it proved necessary to remove it and replace the small mirror by a larger mirror clamped directly to the main optical bench. Subsequent to these modifications, the system stability was verified by generating a filter over the full 4-inch by 5-inch field. Although no attempt was made to optimize the filter recording parameters, the filter reconstructed well over the entire area.

Thermal lensing in the liquid gate was caused by beam heating of the index matching fluid. The laser beam has a Gaussian intensity profile which induces a local thermal profile of approximately the same form. The liquid's index of refraction varies with temperature and in turn produces a lens-like phase shift on the light passing through this region of the gate.

24

The net effect of this phenomena is to induce a significant shift in the position of the Fourier transform plane. This effect was aggravated by a larger than necessary thickness of fluid in the existing liquid gate. For this reason the liquid gate was modified so that the fluid layer was reduced from approximately 0.5 inch to 0.007 inch on either side of the transparency. This change considerably alleviated the thermal lensing problem.

The original system was designed so that the reference beam collimator was also to be used as the inverse transform lens required to form the correlation plane. Furthermore, the correlation measuring devices were mounted on a large extension cantilevered diagonally off a corner of the main optical table. This arrangement was awkward in that it was difficult and time consuming to reposition the large reference beam lens. Moreover, the cantilevered extension limited the positioning of output sensors. Consequently, we removed the extension and used a mirror to redirect the correlation output along an auxiliary optical rail placed at the end of the main table. An appropriate lens was mounted on this rail to form the correlation plane. The vidicon camera mount was also placed on this rail. The reference beam lens was fixed in position.

This set up, which was composed of available in-house equipment, is much more convenient, reproducible and accurate than the original arrangement.

A sensor intended for measuring correlation peak locations was considered inadequate and was replaced by a vidicon camera. In order to avoid problems associated with distortion in the vidicon's scan raster, we adopted the method of measuring the motion of the camera required to center the desired correlation peak on the face of the vidicon tube. Camera position was originally measured using dial indicators (0.001 inch/division). This proved to be relatively coarse and these indicators were replaced with precision linear potentiometers whose resistance (and hence position) was

25

monitored by a pair of digital multimeters. This arrangement provided improved resolution (approximately 1.5μm per least count).

The original telecentric scanner consisted basically of two galvanometers and a pair of lenses mounted on a small optical rail which extended off one side of the main optical table. This arrangement proved difficult to align and was a minor hazard to personnel. Consequently, we designed and built the more compact scanner illustrated schematically in Figure 4-4. The horizontal mirror and the lens form a unit power telescope which images the galvanometer mirrors onto each other. The mirror can be tilted in two axis and translated vertically for alignment and focusing. The lens-mirror combination can be translated vertically for focusing. Each galvanometer can be tilted about two axis perpendicular to the mirror shaft (pitch and yaw). The entire scanner is mounted on a translation stage for positioning with respect to the collimator lens. This device is relatively compact and has proved adequate. The galvanometers themselves, however, suffer from drift, hystresis, and gain changes. Use of thermally compensated galvanometers with position feedback is essential if truly reliable operation is to be achieved.

4.3   OPTICAL SYSTEM ALIGNMENT

Proper alignment and calibration of the system are required in order to produce accurate and repeatable results. This section discusses the basic steps required to align the COMAP system in both the filter generation and data collection (scanning) mode. When properly aligned, the system can quickly be changed from one mode to the other without any need for significant adjustments.

Alignment of the signal beam is somewhat complex while that of the reference beam is comparatively simple. The major steps involved in system alignment are described briefly below. The terms horizontal and
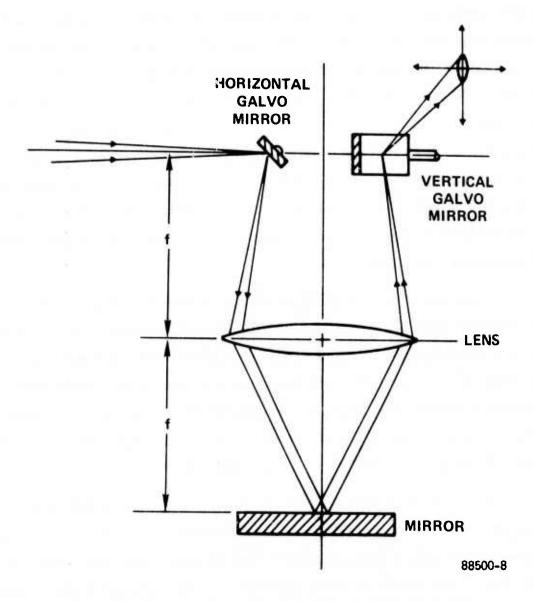
26

FIGURE 4-4.   FOLDED TELECENTRIC SCANNER

88500-8

27

vertical will be used to designate directions parallel and vertical to the surface of the optical bench which may or may not be truly horizontal.

The large Fourier transform lens is first shimmed so that its optical axis is horizontal; any of a number of obvious procedures can be used for this step. All major optical components are placed in their approximate positions, except for the microscope-pinhole assemblies and the reference beam collimator which are temporarily omitted. An auxiliary alignment laser is mounted so that its beam is directed backward through the system (i.e. from the filter plane to the collimator, etc.). This laser beam is made colinear with the optical axis of the large lens by means of the reflections from the surfaces of the lens (Boys' point method of alignment). The signal beam collimator axis is then made colinear with the laser beam using Boys' method. The signal beam routing mirrors and beamsplitter are then adjusted so that the beam from the Argon laser is colinear with that of the alignment laser beam.

The signal beam pinhole assembly is then introduced and adjusted so that the collimator produces a uniform, collimated beam. A convenient method for checking beam collimation is to observe the interference pattern between the front and back surfaces of a high quality beamsplitter. When straight fringes are obtained, the pinhole is at the correct distance from the collimator and the beam is collimated. The signal beam will then be focussed to a point in the center of the filter plane.

The reference beam is then aligned by positioning the necessary mirrors so that the unexpanded Argon laser beam pierces the center of the filter plane. The output routing mirror and inverse transform lens are aligned next. The reference beam collimator is then placed in the system and adjusted so that its optical axis is aligned with the reference beam. The reference beam pinhole assembly is then introduced and aligned to produce a collimated reference beam. The point at which this beam is
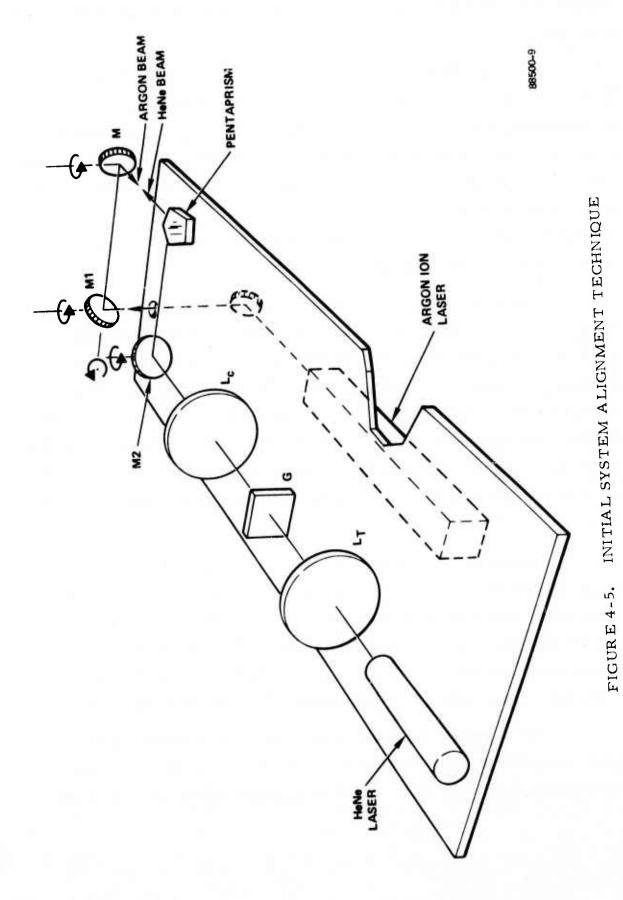
28

focused by the inverse transform lens defines the position of zero parallax (center) in the correlation plane. This completes the filter generation mode alignment.

To align the system for the scanning mode, the arrangement shown in Figure 4-5 is used. The scanning beam routing mirror M_3 is placed between the collimator and the signal beam pinhole, and adjusted to deflect the alignment laser beam 90°. A pentaprism is temporarily used as a convenient substitute for the telecentric scanner. It is placed in the approximate location the scanner will occupy. Mirrors M_1 and M_2 are adjusted to deflect the alignment laser beam at 90° to make the Argon laser beam colinear with the alignment laser beam.

The scanner is initially aligned separately by carefully imaging one mirror onto the other in 514.5 illumination. Then the axis of its horizontal translation stage is aligned so that, as the scanner is translated, the alignment laser beam remains centered on the galvanometer mirror nearest the collimator lens. Mirror M_3 is temporarily removed and an auxiliary mirror and lens used to view the signal beam pinhole through the collimator. Mirror M_3 is replaced and the scanner translated until the galvanometer mirrors focus in the same plane as did the signal beam pinhole.

Mirror M is now translated to bring the Argon laser beam onto the galvanometer mirrors. The scanning beam optics consisting of two microscope objectives and a pinhole are placed between M_1 and M and adjusted to form a beam of the desired cone angle focussed on the galvanometer mirrors. The system is now ready for final alignment. Typically, a 1 mm diameter scanning beam was used (see Figure 4-6).

The alignment laser and mirror M_2 are removed. A microscope is positioned to observe the signal beam focus in the filter plane. A mask having four small holes, one at each corner of the field, is placed
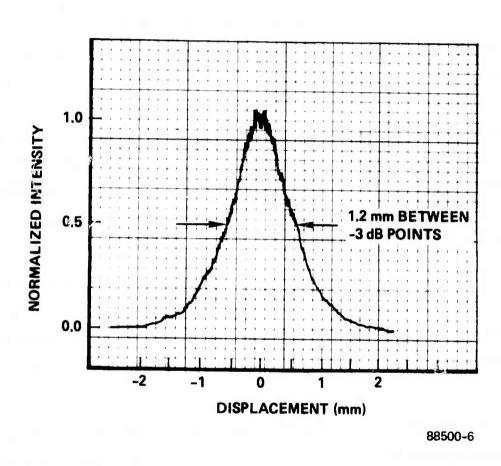
FIGURE 4-5. INITIAL SYSTEM ALIGNMENT TECHNIQUE

30

FIGURE 4-6. INTENSITY OF SCANNING BEAM IN INPUT PLANE

just behind the input gate. This Hartman mask creates four Airy discs at the plane of focus. The microscope is focused so that these four Airy discs overlap exactly; this defines precisely the filter plane. The Hartman test was necessary because of residual spherical aberration in the signal beam (see Appendix B). The filter holder should now be focussed in the filter plane.

The mirror M_2 is replaced for scanner alignment. The galvanometer mirror nearest the collimator is oscillated and the scanning spot observed in the filter plane. The scanner is translated until the spot remains stationary. This assures the final galvanometer mirror is properly focussed into the filter plane. The other galvanometer mirror is now scanned and, if necessary, the galvanometer lens and mirror adjusted until the spot is again stationary. Iterative adjustment of scanner position will be necessary to position the scanning beam spot on the center of the filter plane. A final small correction may be made using the mirror M_2, but this should be minimized or avoided completely.

The scanning beam must be collimated as it passes through the input gate. This is accomplished by adjusting the beam forming optics and pinhole. Since it is difficult to verify the collimation of a 1 mm diameter beam by direct observation, the following procedure was adopted (see Figure 4-7).

The system is put in the filter generation mode and a grating of, say, 50 lpmm is placed in or near the input plane. A photographic plate in the filter holder is exposed to record the spectrum of this grating. To avoid any possibility of space-variant distortion of the spectra, the grating should be covered with a mask limiting its illumination to a small, central region. The photographic plate is developed and replaced in the filter plane. The system is returned to the scanning mode with the grating still in place. The location of the spectral orders are observed with a microscope as the
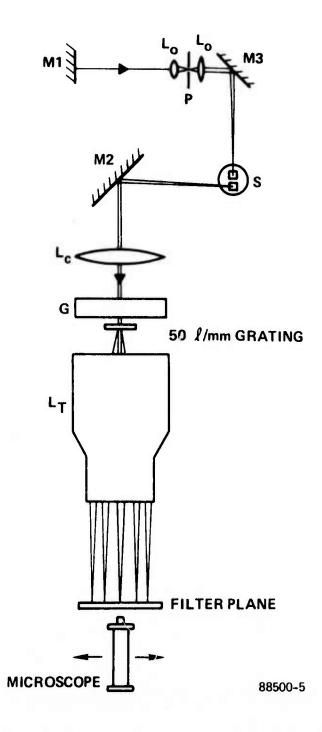
32

FIGURE 4-7. SCANNING BEAM COLLIMATION TECHNIQUE

beam forming optics are adjusted. When the beam is properly collimated, the spectral orders will exactly coincide with those recorded on the plate.

SECTION V

EXPERIMENTAL TECHNIQUES

SECTION V

EXPERIMENTAL TECHNIQUES

This section covers optimization of spatial filter performance, input preprocessing and data collection. Good spatial filter performance is necessary for adequate correlation performance. Fortunately, the filter optimization procedure is straightforward and its performance shows a reasonable tolerance of variations in filter recording parameters. In the course of performing correlation experiments, we found that a form of input preprocessing called "silver masking" considerably improved system performance. We developed parallax data collection procedures which were designed to minimize the effects of certain system insufficiencies. The good agreement between COMAP and AS-11 data indicates that these procedures were successful.

5.1   SPATIAL FILTER OPTIMIZATION

The matched filter, or Fourier transform hologram, is the most important element of the system and its performance determines, to a great extent, the performance of the overall system. Perhaps the principal advantage of a holographic filter is that it performs a true complex cross-correlation. That is, it operates on both the amplitude and phase of the incoming wavefront. A properly recorded filter can be made to exhibit band-pass characteristics and effectively enhance the response of the system to the fine details of photographs; then accurate parallax measurements can be made. That is, a spatial filter can be made which rejects low-frequency information while capturing, faithfully, information associated with edges and details. The frequency band must be carefully selected because we do not wish to lose cross-correlation between corresponding regions due to relatively minute changes in their appearance.

The two most important parameters in the filter construction process are exposure and the ratio of reference to signal beam (K-ratio). One of the light beams impinging upon the photographic emulsion during the filter recording process is the Fourier transform of an aerial photograph. This is a light distribution having its greatest intensity at its center and tapering off rapidly toward the edges. The extent and manner in which this spectrum varies with distance from the center of the filter -- that is, with increasing spatial frequency -- is determined by the characteristics of the input transparency. High-resolution imagery will produce a spectrum which is relatively intense at higher spatial frequencies. If, on the other hand, the input image lacks fine high-resolution detail, more and more of the light will be concentrated toward the lower frequencies. The enormous dynamic range of a spectrum makes it almost impossible to record it all faithfully in a hologram. The reason for this can be seen by recalling that the hologram is essentially a recording of the intensity of the light pattern created by the interference of two beams. If these beams are of equal intensity, the fringes created by them will tend to have 100 percent modulation. If, however, one of the beams is considerably stronger than the other, the depth of modulation of the fringes will be correspondingly less. Finally, because of the limited dynamic range of real photographic emulsions, beams of extremely different intensities will produce fringes of such low modulation that they will be lost in the noise of the emulsion itself. That is, the reference beam can be adjusted to maximize the modulation of the interference fringes only over a limited region of the spatial frequency domain. However, this will mean sacrificing other regions of the frequency domain.

In general, the low-frequency information contained in an aerial photograph is not useful in obtaining high-quality cross-correlations. Consequently, a spatial filter should be recorded to maximize its response at higher frequencies and to minimize or suppress its response at low spatial frequencies. This is done simply by adjusting the reference beam to a

37

value which matches approximately the intensity of the spectrum in a spatial frequency band of interest. The photographic emulsion is exposed to optimize the exposure in the spatial frequency regions of interest. This normally results in overexposure of the low-frequency region of the spectra producing a filter which has little, if any, response in this region. The bandpass characteristics desired in a spatial filter are determined, to a great extent, by the application and the characteristics of the imagery to be correlated. Typically, in a photogrammetric application, it is unnecessary to pass any frequencies lower than the reciprocal of the diameter of the scanning beam. It is also unnecessary, and even undesirable, to pass frequencies which extend beyond the practical resolution of the stereo imagery.

An experiment was performed with a typical aerial photograph to optimize the exposure for a matched spatial filter. A series of spatial filters were made where the exposure was varied from 40 to 1280 $\mu J/cm^3$ and the signal-to-noise ratio (SNR) of the correlation peak was measured along with the diffraction efficiency. Figure 5-1 shows a graph of the results where the exposure is plotted versus signal-to-ratio and the diffraction efficiency of the correlation peak. Note the peak SNR and the peak diffraction efficiency occur at approximately 80 $\mu J/cm^2$ exposure which is nearly the exposure needed to produce an amplitude transmittance of 0.5 for an amplitude hologram. Therefore, all the exposures were kept at approximately 80 $\mu J/cm^2$.

In this and all subsequent measurements, the SNR is defined as the peak signal intensity to average noise intensity where the noise is defined as any light in the output plane which is not contained in the actual correlation peak. The noise is composed of the cross-correlation of the filter impulse response with the input scene, scattering due to the nonlinear characteristics of the filter, and grain noise effects. Of these, the cross-correlation component is generally the most significant.
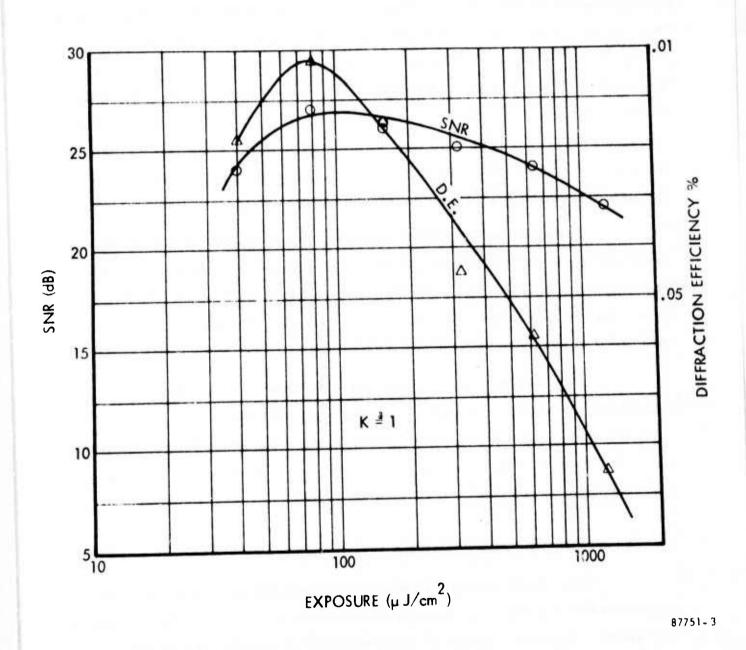
38

FIGURE 5-1.   SNR AND DIFFRACTION EFFICIENCY vs. EXPOSURE

87751-3

Another experiment was performed to optimize the reference-to-signal beam ratio (K-ratio) for a typical aerial photograph based on the SNR produced at the output of the optical system. A series of six filters was made where the K-ratio was $\frac{1}{4}$, $\frac{1}{2}$, 1, 2, 4, 8; each filter was exposed by approximately 80 $\mu J/cm^2$. The SNR of the resulting autocorrelation peak was measured by means of a scanning photomultiplier with an 18μ by 180μ sampling slit; a 30-inch f/5 lens was used as the inverse transform lens. Figure 5-2 shows a graph of the SNR of the correlation peak as a function of the K-ratio, for two beam sizes. Note that for a 5-7.5 ℓpmm bandpass annulus used to measure the K-ratio, a steady increase in SNR is observed for higher K-ratios; this means that the most significant contributions from the image occur at spatial frequencies under 5 ℓpmm.

The above optimization experiments were performed with conventional copies of aerial photographs. Subsequent experiments with preprocessed imagery (see Section 5.2) produced similar results. In this latter case, a reference beam exposure of 46 $\mu J/cm^2$ and a K ratio of 2 measured over 2.5-5 ℓpmm was taken as optimum.

It is important to note that filter performance is relatively tolerant to variations in K ratio and exposure. While it is desirable to approach the optimum for recording parameters, a practical range of values can be accepted. Consequently, automatic control of the filter-making operation should be relatively easy to implement.

5.2   INPUT PREPROCESSING

Edge detail contrast in an aerial photograph is one of the most important factors affecting the correlation performance of a coherent optical correlator. Between regions of equal resolution, those areas having greater edge detail contrast will usually produce correlation peaks with a better signal-to-noise ratio than do areas of less edge contrast. High
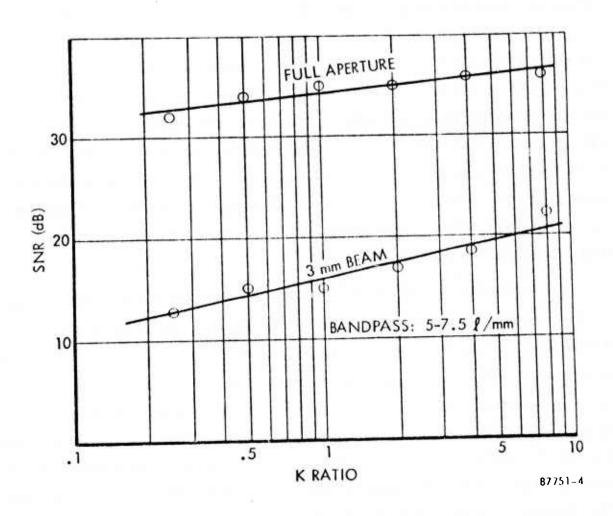
40

FIGURE 5-2. SNR vs. K-RATIO

87751-4

contrast regions not only have more energy in the spatial frequency bands most important in matched filter correlation, they also produce less scattered noise due to film grain.

A major difficulty in obtaining good correlation response over an entire frame is that gross tonal variations use the major part of the transmission range of the recording material and edges cannot be recorded at maximum contrast throughout the entire frame. That is, to record detail in scenes which have areas ranging in tone from bright to dark, relatively low gamma films are used. This approach preserves detail throughout the entire scene, however, it means that edge contrast is low, especially in regions which differ significantly from the average brightness of the scene. The original aerial photo cannot be simply copied on a high contrast film in order to enhance edge contrast because this would cause a loss of detail in some regions. However, by using local dodging, a high contrast emulsion can be used in making a copy which has great edge contrast while preserving detail throughout the picture.

We made copies of the Canadian test model transparencies using a "silver mask" technique to provide local dodging. The original glass diapositives, which have very low contrast, were placed in contact (emulsion to emulsion) with an unexposed photographic plate having a high contrast emulsion. A negative copy (the silver mask) of the diapositive was placed on top of the diapositive. A small, distant light source was used to expose the plate through the combined positive/negative transparencies. The negative transparency casts a somewhat unsharp shadow on the emulsion of the dispositive. The diapositive in turn casts a very sharp shadow onto the unexposed plate. On a gross scale, the transmissions of the positive and negative tend to cancel each other and produce an almost uniform exposure. However, the sharp edge detail of the diapositive is not cancelled since the shadow of the negative is not sharp. Hence, edge detail and contrast is preserved while

42

gross tonal variations are smoothed out. Proper exposure and development of the high contrast plate produces a transparency with good detail and high edge contrast throughout.

Three masking techniques were used to prepare three sets of edge enhanced stereo pairs. The masks were negatives, printed on a film with $\Gamma = 1$ from the original diapositive. The unity gamma allowed the negatives to be complementary in density to the original scenes. The techniques used to construct the masks caused differeing amounts of spatial frequency content to be recorded. The masks, in order of decreasing spatial frequency content, are denoted as Type 1, Type 2, and Type 3. The Type 1 masks were contact printed from the original master scenes with the film emulsions on the outside of the film sandwich. Thus, loss of resolution was introduced by the thickness of glass between the emulsions. Type 2 masks were constructed similarly, except a weak diffuser was also inserted between the plates, causing further loss of resolution. Type 3 masks were exposed through an enlarger to a slightly defocussed, but one-to-one, image of the master scene. Type 3 masks proved to have artifacts induced by the out-of-focus condition.

After a number of trials using these masks, we succeeded in making copies of the Canadian Model having the desired resolution and contrast. The Type 1 mask appeared to produce the best results. Some of these transparencies were used to make spatial filters in the usual manner. Their auto and cross-correlation performance proved to be markedly better and more uniform than that obtained using conventional transparencies. It was possible to obtain useful correlations in many areas where such had not been obtained in conventional copies of the same scenes.

An artifact observed when using these silver mask copies is the presence of an occasional satellite peak adjacent to the true cross correlation peak. This may be a result of a shadowing effect caused by slight

misregistration of the silver mask. In any case, this satellite peak is always relatively weak and could not be confused with the true correlation peak.

Figures 5-3 through 5-5 illustrate the effect of silver mask copies. In these figures, we have attempted to depict as accurately as possible the appearance of transparencies used in this experiment. The prints are the same polarity as the actual transparencies. Figure 5-3 shows the original low contrast, high resolution diapositive. The areas labeled A, B, and C are regions of increasing average transmission. A typical high contrast transparency is shown in Figure 5-4. While this copy has greater edge contrast and good resolution in many areas (e.g. Region B), other regions are overexposed (A) or underexposed (C) and have lost information. A transparency made with the silver mask technique is shown in Figure 5-5. In this case there is good resolution and contrast throughout the frame despite its somewhat unnatural appearance. In particular, Region B still has good contrast and detail while Region C shows strong edge detail which was originally of low contrast in Figure 5-3 and completely lost in Figure 5-4. Although it is not apparent on the print, the contrast of detail in the dark region (A) is also improved; clear areas are now visible between trees.

Our results indicate that high contrast, high resolution copies of aerial photographs improve correlation performance in a coherent optical system. (They would probably have a similar effect if used in an electronic correlation system such as the AS-11B). Producing such copies is undesirable in that it represents an additional step in the photogrammetric process. However, what we have done here is merely an extreme case of local dodging. Consequently, the production of such copies should not present any major operational problems since continuous strip contact printers having automatic dodging capability are well developed and commercially available.
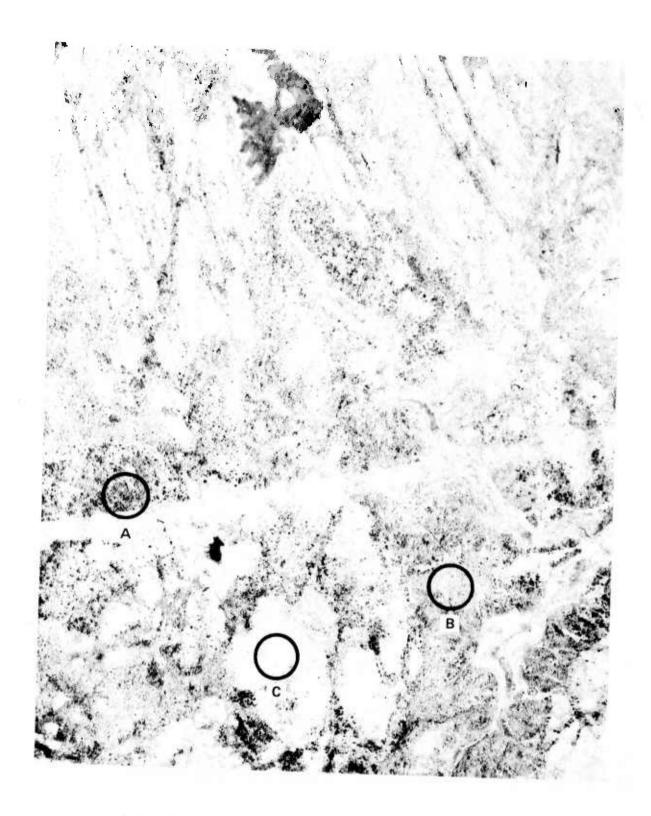
44

FIGURE 5-3. ORIGINAL AERIAL PHOTOGRAPH

FIGURE 5-4.   HIGH CONTRAST COPY

FIGURE 5-5.   SILVER MASK COPY

SECTION VI

DATA COLLECTION

SECTION VI

DATA COLLECTION

Several steps are involved in collecting parallax data. The scanner and correlation peak position measuring device must be calibrated. The input transparency must be properly oriented and the relation between photo and scanner coordinates established. The actual data collection operation must be planned to minimize systematic errors.

6.1   SCANNER LINEARIZATION AND CALIBRATION

The scanner presently in the COMAP System is inherently non-linear. That is, beam position in the input gate is a non-linear function of the voltage applied to the input of the galvanometer drivers. While this non-linearity could be corrected during photogrammetric reduction of the data, we considered it more desirable to linearize the scanner. This had two advantages: first, it simplified subsequent data reduction, and second, it allowed operation directly in photo coordinates which is important because it greatly simplifies addressing control points.

In the initial calibration and during all subsequent use of the scanner, it was necessary to minimize the effect of galvanometer hystresis. Addressing the same point in the input from opposite directions typically resulted in an error on the order of 2 mm (3 mrad).

This intolerable hystresis effect is avoided by resetting the scanner to a specific point far off one corner of the field before addressing any location in the input. This procedure is simple to implement with the galvanometers under computer control and was always used.

Linear scanning was achieved in a two-step process. First, a photographic plate was placed in the input plane and exposed to the scan

produced by a series of equally incremented digital values sent to the D/A converters by the computer. The positions of the spots on this plate were measured, producing a set of ordered pairs consisting of the digital addresses and their corresponding displacements in the input plane. A third order polynomial was fitted to these values. The computer was then programmed so that any point in the input plane can be addressed directly by its photocoordinates in millimeters. This capability of addressing directly in photocoordinates proved to be a considerable convenience for finding reseaus and control points in the input scene.

Repeatability of the linearization was hampered by galvanometer zero drift and gain change. These effects were not large enough during a data collection run to cause serious problems. Zero drift typically caused a 0.2 mm offset over one hour. Gain changes manifested themselves over longer times, causing typically a 5 percent scale change in a 24 hour period. Updating of the third order polynomial fit by altering the linear coefficient to accommodate the new galvanometer parameters was implemented to account for small changes. Operating the scanning system in a closed loop or self-calibrating method would eliminate changes caused by zero drift and gain changes, thus guaranteeing both linear and repeatable scanning.

6.2   INPUT ALIGNMENT

Correct alignment of the input transparency in both orientation and position maximizes the average cross correlation signal-to-noise ratio and minimizes the parallax range. These are both desirable goals. Consequently care was taken to ensure good alignment. In the Canadian Test Model frames, there is very little rotation between scenes (the yaw angle η is small) and we decided to use reseaus for alignment. Where there is significant rotation between frames, the input must be oriented on the basis of selected points in the scene.

50

Alignment is achieved by using the holographic property of the spatial filter to allow simultaneous viewing of the frame used to make the filter and the frame presently in the input. To do this, an auxiliary lens is placed just after the filter and colinear with the signal beam axis. This lens is selected so that it, in conjunction with the Fourier transform lens, will form an aerial image of the input at some convenient scale and location. This image can be viewed directly or with the aid of a microscope. The system is placed in the filter generation mode and the reference beam allowed to illuminate the filter. This produces a holographic reconstruction of the input used to make the filter. To an observer viewing through the microscope, this original scene appears to be present in the input gate.

Blocking the reference beam and letting the signal beam to pass will allow the observer to see the scene actually in the input gate. Simultaneous presence of the reference and signal beams produces superimposed images which greatly simplify alignment. We used this technique to precisely align the reseaus of the frames being cross correlated.

The scanner coordinates are converted into photocoordinates by locating a particular reseau (commonly the master reseau) and using this information to determine the transformation between photo and scanner coordinates. The computer program then allows the operator to directly input photo coordinates.

6.3   DATA RUN CALIBRATION PLATES

As a check of system consistency and performance, a calibration plate was made before and after each data. This consisted of placing an unexposed photographic plate in the input and stepping the scanning beam along the desired scan path in relatively large (2 mm) intervals. The beam was also sent to a number of control points. The resulting plate has a series of spots which can be used to verify the consistency and accuracy of the scanner

51

in tracking properly along the scan and in properly addressing control points. These plates were made relatively easily and quickly under total computer control.

6.4 PARALLAX DATA COLLECTION

Parallax data is collected by scanning the beam through known locations on the input plane while monitoring the position of the cross correlation peak in the output plane. Parallax values are collected for control points where ground elevation is known and along the scan line for which a profile is to be generated. Typically, two hundred 0.5 mm steps constitute a scan. Parallax at from ten to twenty control points is measured with each scan.

A vidicon camera located in the output plane displays the correlation plane on a television monitor. Also shown on the television monitor is a pair of fixed electronic crosshairs. The position of the correlation is determined by displacing the vidicon camera until the correlation peak appears directly under the electronic crosshairs. Two linear precision potentiometers attached to the translation stages that displace the vidicon are used to measure displacement. Two digital voltmeters operating in a ratiometric mode display the voltage ratio across the potentiometers. The displacement measuring system has a 1.5μm precision and is linear to at least 0.15 percent over the typical displacement range. The lack of geometric fidelity of the vidicon, thermal drift of the galvanometer drivers, the drift of the electronic crosshairs, and the inability to precisely locate the position of the correlation peak presently affect the accuracy obtained for the correlation position measurement.

To monitor galvanometer drift, the scanning beam is periodically sent to a particular reseau which is projected onto a screen by a fixed microscope. The reseau is chosen so that the microscope can be left in

position during a complete data run without blocking the scanning beam.
A typical projected view of a reseau is shown in Figure 6-1. In this case,
the galvanometer has drifted so that the scanning beam is approximately
0.5 mm low. This is a negative transparency and the black cross just below
the reseau is a control point marked on the ground with white paint.

During parallax data collection, the operator records the location
of the scanning beam and the correlation position readings from the digital
voltmeters. He also observes the monitor and makes a subjective estimate
of the quality of the correlation peak ranging from poor to excellent. Typical
video signals associated with correlation peaks of various subjective
qualities is shown in Figure 6-2. The horizontal scale is $660\mu m$/division
and a correlation peak is less than $100\mu m$ wide at its half power points. The
maximum of the correlation can readily be determined to within $\pm 20\mu m$.
This type of oscilloscope display was not used for data collection; only the
monitor-crosshair display was used.

6.5   BEAM DITHERING

We found that, in regions where the correlation signal-to-noise
ratio was low, significant improvement in signal-to-noise could be obtained
by dithering the beam. That is, the beam was rapidly moved to a series of
locations around the nominal beam position. The locus of these points was
at a radius of one half beam diameter (≈ 0.5 mm) from the nominal position.
This simulates, to some extent, the use of a larger beam. The effect of
dithering is illustrated in Figure 6-3.

This technique proved to be extremely useful while collecting
parallax data. The computer was programmed so that the operator could
request beam dithering at any time as the computer stepped the beam across
the scan line. In a number of instances, adequate correlation peaks were
produced where a very poor peak or none at all could be observed with a
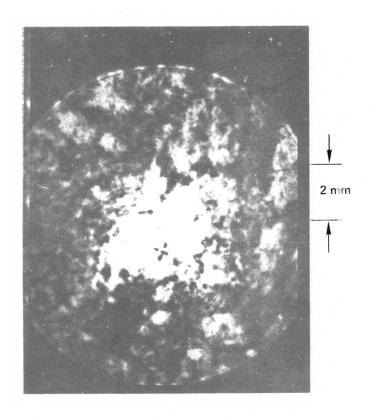stationary beam.

53

2 mm

FIGURE 6-1.   RESEAU AND CONTROL POINT ILLUMINATED
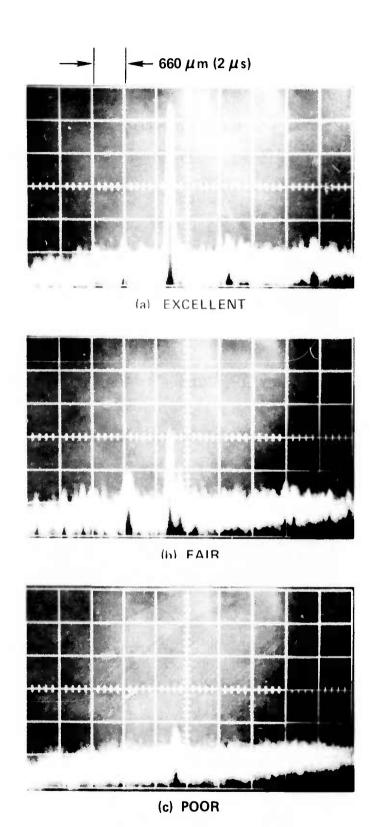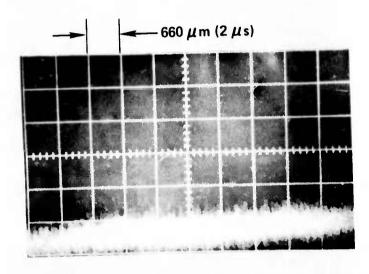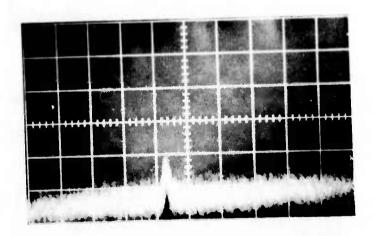BY SCANNING BEAM

660 µm (2 µs)

(a) EXCELLENT

(b) FAIR

(c) POOR

FIGURE 6-2.   VIDEO SIGNALS CORRESPONDING TO
CORRELATION PEAKS

$\longleftarrow$ 660 μm (2 μs)

(a) CORRELATION PROFILE WITHOUT DITHERING

(b) CORRELATION PROFILE WITH DITHERING

FIGURE 6-3.   EFFECT OF SCANNING BEAM DITHERING

56

Beam dithering improves correlation performance by means of two effects. First, the beam sweeps out a larger area, thus increasing the probability that some details capable of yielding a good correlation will be illuminated. Second, the process tends to incoherently sum the desired correlation peak over all these beam positions while averaging the noise. That is, for each beam position, noise peaks occur at slightly different locations in the output while the desired correlation peak always tends to appear in the same place.

This technique has produced such significant results that it should be considered as an adjunct or possible replacement for beam size control in a COMAP system. Besides its apparent effectiveness, it has the advantage of requiring no additional components and practically instantaneous response. Beam size controls which involve moving lenses or an iris will be slower.

6.6   DATA COLLECTION PROGRAM

The operation of the data collection program is indicated schematically in the flowchart of Figure 6-4. The program was written in a modified version of "Focal," a ligh level language commonly used on Digital Equipment Corporation's PDP8 series of minicomputers.
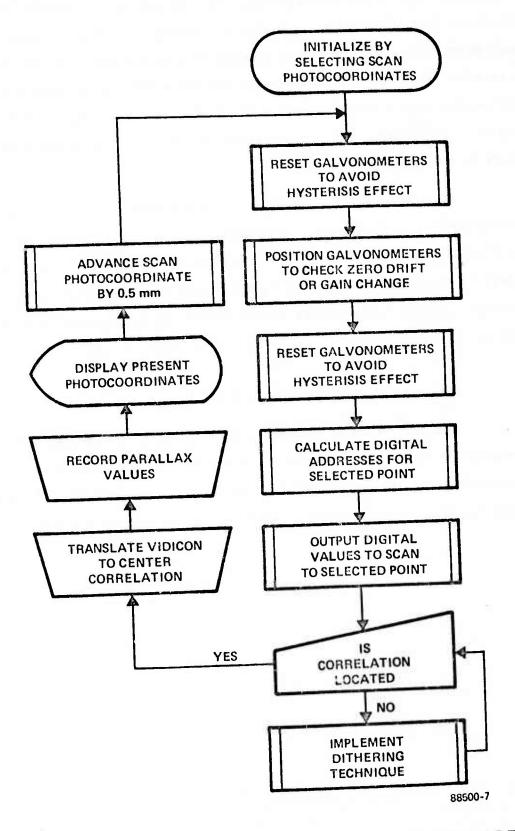
57

FIGURE 6-4.　DATA COLLECTION PROGRAM FLOWCHART

SECTION VII

DATA REDUCTION AND EVALUATION

DATA REDUCTION AND EVALUATION

Photogrammetric data reduction and evaluation were performed by DBA, Inc., Melbourne, Florida. Data collection runs were made from time to time during this program. Each complete set of data was promptly reduced and plotted along with the corresponding parallax profiles derived from AS-11B data. Results were discussed and necessary modifications in equipment or procedures determined. The consistency and accuracy of the data improved with each data run until the last several sets of parallax data showed excellent agreement with AS-11B parallax profiles.

7.1   DATA REDUCTION

Data reduction procedures were developed and modified as necessary as the effort progressed. The methods employed were not strictly rigorous, but seemed to be the best approach in view of the current hardware restrictions.

A mathematical model of the AS-11B system was developed and used to compute AS-11B parallaxes and ground point coordinates. The AS-11B stereo-model parameters from the Canadian shutdown tape, supplied by RADC, were entered in DBA's analytical model and derived ground point coordinates were checked against the supplied control values. Twenty points which were read as AS-11B setup points had one sigma value with respect to the known control of .11 meters in x, .15 meters in y, and .32 meters in z (approximately 12μ).

The parallax values for points within the model were computed in the following manner: (1) using the analytical AS-11B model the correct object space coordinates, and the photo coordinates for all control points and profiles were computed; (2) the φ and ω angles were set equal to

60

zero; (3) an arbitrary point was selected (control point (30)); and the "y" coordinate of the exposure station for photograph two was translated until this point had zero "y" parallax; (4) the photo coordinates for all points were then computed using this model orientation with the elevation of all points being considered as that of (control point 30) the arbitrary reference point; (5) the difference between the two sets of photo coordinates was defined equal to the parallax relative to the chosen reference.

The image correlator data was reduced in the following manner: (1) the output parallaxes were scaled by appropriate constants to transform them to an absolute system, .48638 for P_x and .62073 for P_y;[*] (2) the output x, y coordinates were transformed into the AS-11 model coordinate system, using a linear conformal transformation; (3) the parallaxes, as read on the control points within the image correlator model area (approximately 20 points), were adjusted into the parallaxes as derived on the corresponding points from the AS-11 analytical model; (4) the x_p and y_p adjustments were computed separately using a least squares adjustment of the following equations:

$$P_x' = P_x + a_0 + a_1x + a_2y \quad \text{and} \quad P_y' = P_y + b_0 + b_1x + b_2y,$$

where P_x' was the AS-11 derived parallax during the least squares solution for a_0, a_1, and a_2 and became the derived parallax when the equation was evaluated. P_y' was found in the same manner; (5) this adjustment effectively adjusted the planes of the two parallaxes together; (6) the results were plotted on a calcomp plotter, the vertical axis being either x or y parallax while the horizontal axis was the y positional coordinate.

---

[*] See Appendix A for an explanation of why the parallax scales differ between x and y.

7.2 EXAMPLES OF PARALLAX DATA

The stereo pair showing the Canadian Photogrammetric Test Range are shown in Figures 7-1 and 7-2. Only the overlap region is shown and the path of the last four data collection scans on the COMAP system are indicated. The scans are numbered in chronological order and the center of the model coordinate system is shown.

Figures 7-3 through 7-6 present comparisons of parallax data measured on the COMAP system with derived AS-11B parallaxes. These examples correspond to the lines in Figure 7-2 and are in chronological order. In all cases, COMAP data is a solid line and the AS-11B profiles are dashed. The vertical axis represent x or y parallax, and the vertical scales vary from figure to figure. The horizontal axis is the y position of the scanning beam. A number of other data runs were made prior to the four shown here.

In general, the curves show very good agreement. When rotational and translational biases are removed, the agreement is excellent; especially considering the limitations of the present COMAP hardware. It should be noted that the nominal centers of the scans in the COMAP system never exactly coincide with the AS-11B scans. The distance between the x values for COMAP and AS-11B data varies from 50 to 200μm; the AS-11B scans are 750μm apart. This difference between the COMAP and AS-11B scan positions is undoubtedly the cause of some of the difference between curves.

Figures 7-3 and 7-4 represent data obtained using dial indicators with a minimum graduation of .001" (25μm) to measure vidicon position. The relatively crude graduation of these indicators accounts for some of the coarseness in the COMAP data. Figure 7-4 also shows an interesting phenomena which led to a change in data collection procedures. There is a sawtooth pattern to the COMAP data caused by frequently reading sequential
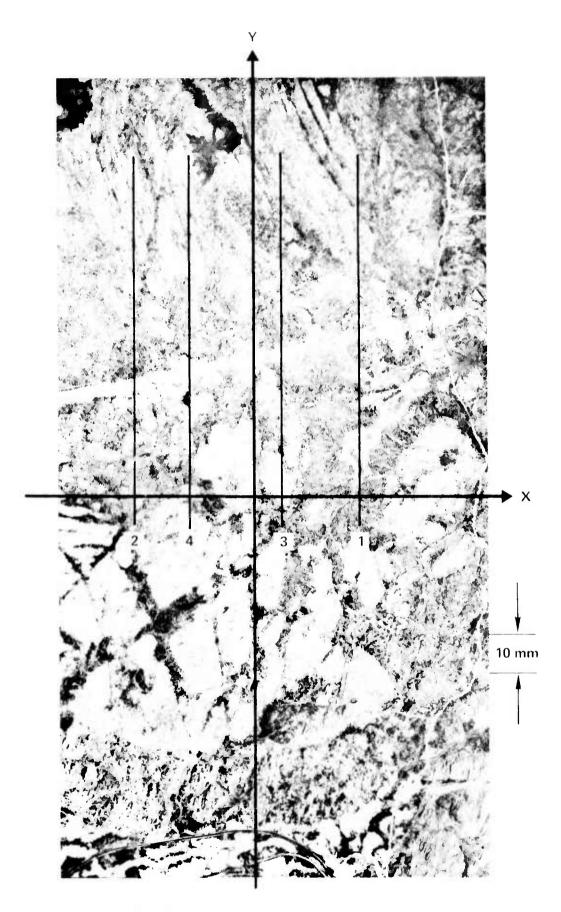
FIGURE 7-1.　CANADIAN TEST MODEL PLATE #1

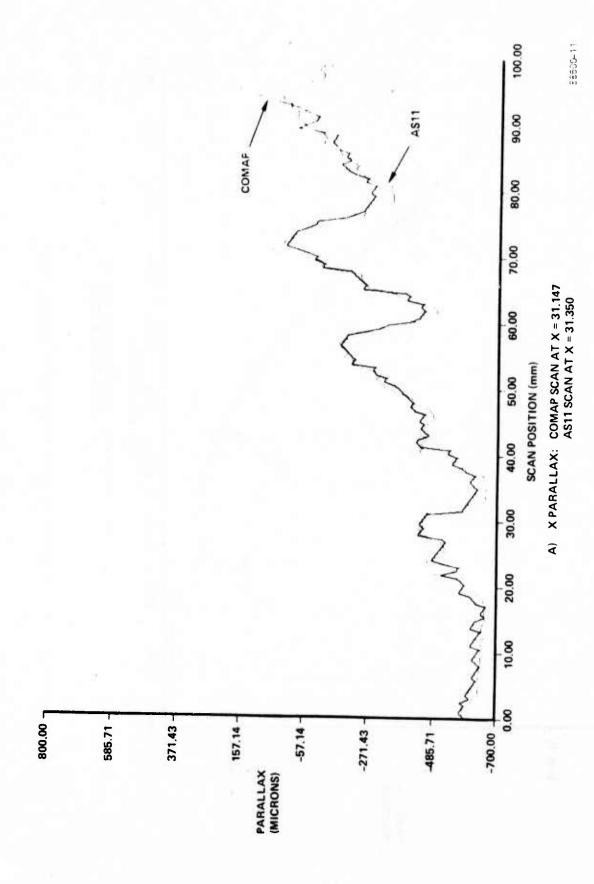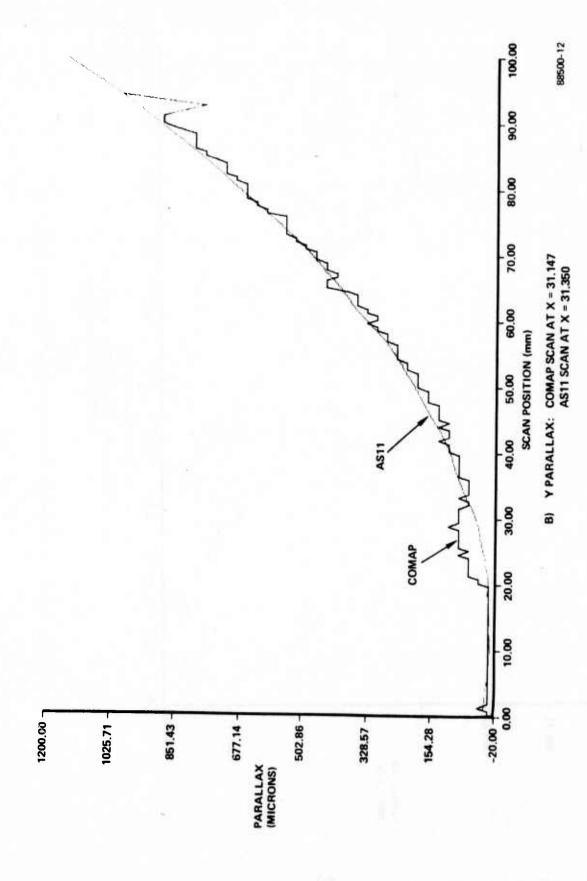FIGURE 7-2.   CANADIAN TEST MODEL PLATE #2

64

PARALLAX
(MICRONS)

SCAN POSITION (mm)

COMAF

AS11

A) X PARALLAX: COMAP SCAN AT X = 31.147
AS11 SCAN AT X = 31.350

FIGURE 7-3a. COMAP & AS11 PARALLAX DATA, SCAN 1

65

FIGURE 7-3b. CCMAP & AS11 PARALLAX DATA, SCAN 1

PARALLAX (MICRONS)

SCAN POSITION (mm)

B) Y PARALLAX: COMAP SCAN AT X = 31.147
AS11 SCAN AT X = 31.350

AS11

COMAP

88500-12
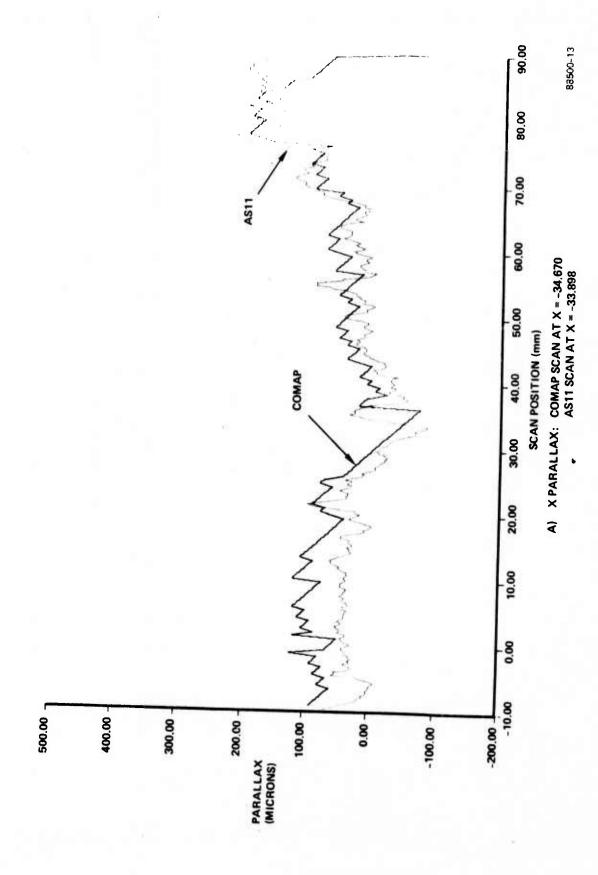
FIGURE 7-4a.   COMAP & AS11 PARALLAX DATA, SCAN 2

A) X PARALLAX: COMAP SCAN AT X = -34.670
                 AS11 SCAN AT X = -33.898

88500-13

67

PARALLAX
(MICRONS)

SCAN POSITION (mm)

AS11

COMAP

B) Y PARALLAX: COMAP SCAN AT X = -34.670
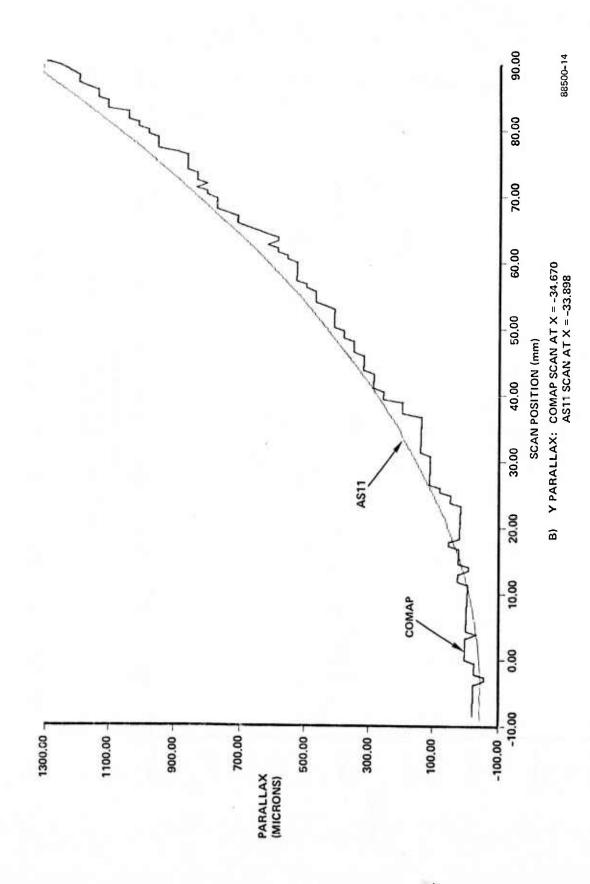AS11 SCAN AT X = -33.898

88500-14

FIGURE 7-4b. COMAP & AS11 PARALLAX DATA, SCAN 2

68

positions of the correlation peak as being identical. There was some rotation between the scenes being cross correlated so that reading the same correlation peak position over several sample points produces a parallax curve having a constant slope.

This is primarily a psychological phenomena in that an observer watching the TV monitor tended not to notice small changes in the correlation peak position when the peak was already almost centered on the electronic crosshairs. Because of this, we adopted the procedure of intentionally displacing the vidicon camera at each sample point so that the correlation peak was well clear of the crosshairs. The correlation was then brought back to the crosshair intersection and vidicon camera position recorded. The new procedure effectively eliminated this "same as before" problem in subsequent data collection operations.

Another interesting feature of Figure 7-4 is the fit between COMAP data is better for larger values of scan (y) position than at lower values. The great majority of control points used in this case were located between y 40 mm and y 100 mm. Because of this weighting, the adjustment of COMAP data into the AS-11B system forced a better fit at this end of the scan. Care was taken in later efforts to provide a more uniform distribution of control points.

Despite the problems involved, the data in Figures 7-3 and 7-4 show good agreement between GOMAP and AS-11B parallaxes. The difference in regions of better fit are quite small and even in regions of worst fit, the average difference is 50µm or less. Some of the difference between the curves is a result of the noncoincidence of the COMAP and AS-11B scan paths.

Figure 7-5a shows data collected using improved resolution in the vidicon camera position measurement. The COMAP data has good detail and follows essentially all of the terrain's undulations. However,
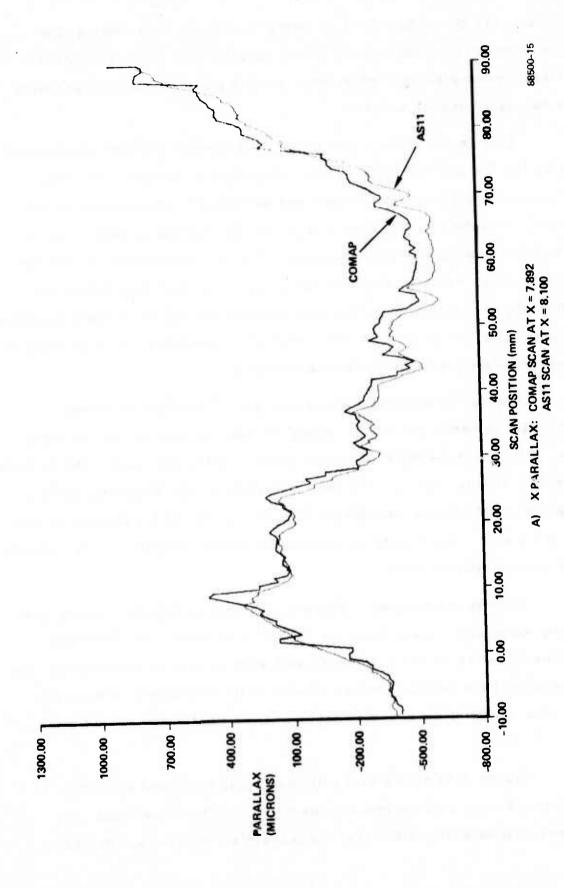
69

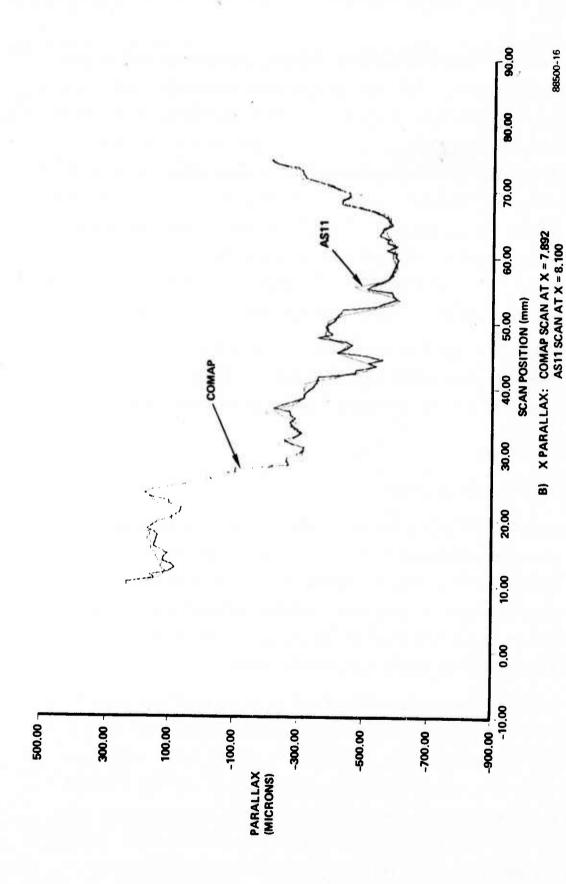FIGURE 7-5a. COMAP & AS11 PARALLAX DATA, SCAN 3, ORIGINAL DATA

A) X PARALLAX: COMAP SCAN AT X = 7.892
AS11 SCAN AT X = 8.100

SCAN POSITION (mm)

PARALLAX (MICRONS)

88500-15

70

FIGURE 7-5b. COMAP & AS11 PARALLAX DATA, SCAN 3,
ROTATIONAL AND TRANSLATIONAL BIASES
REMOVED

B) X PARALLAX: COMAP SCAN AT X = 7.892
AS11 SCAN AT X = 8.100

88500-16

71

there is an obviously increasing difference between the curves with larger values of scan position (y). This implies that there was some residual rotation between the scenes being correlated. A computer program was used to determine this rotation and to recalculate the COMAP data with any rotational and translational biases removed. The recalculated parallaxes are plotted in Figure 7-5b which shows an excellent fit between the COMAP and AS-11B curves. A portion of the data at both ends of the scan was not recalculated and is omitted. Note that the scale of Figure 7-5b is 200μm/ division while that of 7-3a is 300μ/division. Differences between the curves are, therefore, emphasized in Figure 7-5b as against Figure 7-5a.

Figures 7-6a and 7-6b show a similar situation. While the fit between COMAP and AS-11B data is good in 7-6a, it is considerably improved when translational and rotational biases are removed as in Figure 7-6b.

7.3 EVALUATION OF DATA

The data ultimately produced by the COMAP system shows remarkably good agreement with that produced by the AS-11B. The fit between the curves shown in Figures 7-3 through 7-6 is very good, especially considering that the scan paths between COMAP and AS-11B were between 50μm and 200μm apart in all cases. There is also uncertainty of at least 10μm in the AS-11B data itself.

The last two data sets (Figures 7-5 and 7-6) were numerically analyzed to find the r.m.s. difference between COMAP and AS-11 data. The results are tabulated in Table I, which shows that r.m.s. differences of approximately 40μm to 60μm resulted when rotational and translational biases were removed. In both these cases, relatively small intervals near the ends of the scans contribute a great deal to the rms difference. This is due to a few extreme points and steep slopes. A significant source of
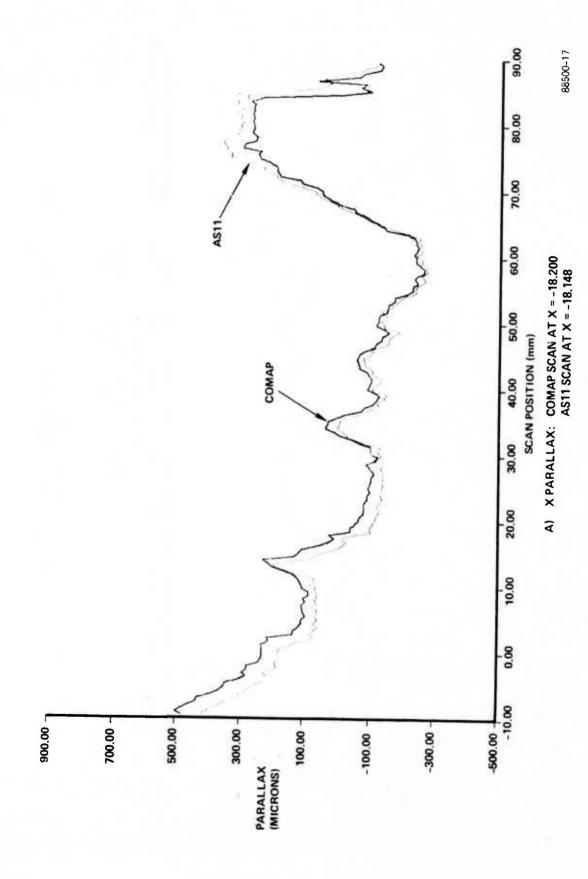
A) X PARALLAX: COMAP SCAN AT X = -18.200
AS11 SCAN AT X = -18.148

FIGURE 7-6a. COMAP & AS11 PARALLAX DATA, SCAN 4
ORIGINAL DATA

88500-17

73

PARALLAX
(MICRONS)

SCAN POSITION (mm)

B) X PARALLAX: COMAP SCAN AT X = -18.200
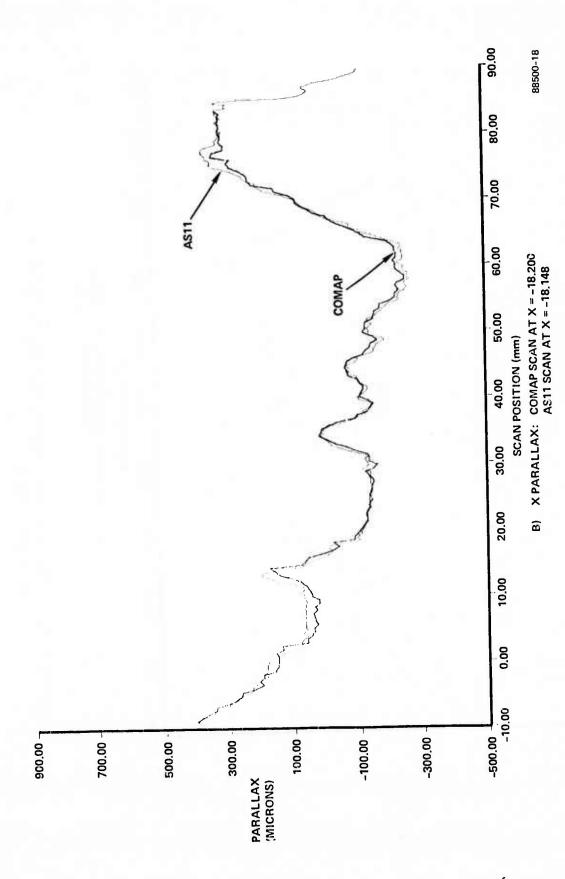AS11 SCAN AT X = -18.148

88500-18

FIGURE 7-6b. COMAP & AS11 PARALLAX DATA, SCAN 4
ROTATIONAL AND TRANSLATIONAL BIASES
REMOVED

74

error in regions of steep slope is the inaccuracy in the galvanometer scanner. The r.m.s. error achieved when some suspect data is edited out is also listed in Table I. Ignoring a small region (14 mm) in Figure 7-6 near a precipitous cliff reduces the r.m.s. difference between COMAP and AS-11B data to 24μm in x parallax. The position of the cliff varies rapidly with x and even a small difference between COMAP and AS-11B scan paths can introduce large differences in parallax.

We feel the COMAP system has yielded results of remarkable accuracy, considering the hardware limitations of the present system.

TABLE I

RMS VALUES (μm) FOR DATA SETS 3 AND 4

Scan Interval (mm) Set #3	Raw Data Adj. to Control		Translational Bias		With Bias Removed		With Rotational Bias Removed	
	P_x	P_y	Bias X	Bias Y	P_x	P_y	P_x	P_y
Unedited -9.351→96.708	78.4	81.1	47.9	-47.2	62.1	65.9	56.5	56.7
Edited 10.030→74.635	78.7	94.8	68.3	-77.3	39.0	54.8	30.1	20.9
Set #4								
Unedited -9.384→97.002	63.2	40.6	13.0	- 3.5	61.9	40.4	40.8	37.5
Edited -9.384→83.569	52.5	38.9	24.2	.4	46.6	38.9	24.2	37.2

SECTION VIII

SYSTEM PERFORMANCE

SECTION VIII

SYSTEM PERFORMANCE

There are a number of factors which will determine the feasibility of an automatic stereocompilation system. These include speed, accuracy, cost, data format, complexity, capability and convenience. We feel a COMAP-type system has the potential for cost effective operation and may offer significant advantages including the ability to be configured into a compact and rugged field unit, especially where smaller format (5" and 70 mm) imagery is involved. The following discussion covers factors relevant to potential system performance and includes an estimate of system performance. Advantages and problem areas are pointed out.

8.1   ACCURACY

The accuracy of any automatic stereocompilation system employing cross-correlation is ultimately limited by the resolution of the imagery. The sharpness and the accuracy with which the center of a correlation peak can be located is determined by the maximum useful resolution of the imagery. A pair of low resolution images will produce broad, poorly defined correlations, while the opposite is true for high resolution imagery. In systems employing image sampling techniques (such as a digital correlator), effective resolution is limited by the resolution and accuracy of the sampling system. (It should be noted that sampling scan jitter will cause an effective loss of resolution as far as cross correlation is concerned, since sample values will not appear in their proper location).

Parallax measurement accuracy will be limited by the effective overall resolution of the system performing the cross correlation. A coherent optical processor (COMAP) can readily be designed and built with an overall resolution exceeding that usually achieved in aerial photography.

The present COMAP optics are designed for 200 lpmm imagery and a different system configuration may allow even greater resolution with simpler and less expensive lenses. Hence an optical correlator should be able to measure parallax to the accuracy limits imposed by the imagery. On this basis, the accuracy of an optical correlator should equal or exceed that of an electronic (digital) correlator.

In order to achieve this parallax accuracy in practice, scanning beam pointing and correlation peak location must be done with suitable precision. The experimental results presented in Section 7 demonstrate that the present COMAP hardware is capable of yielding rather accurate parallax data. A considerable increase in scanner and correlation peak location accuracy can be accomplished by relatively straightforward hardware improvements. Thus, it is reasonable to conclude that a COMAP-type system can measure parallax to the limit of the accuracy imposed by the imagery itself.

8.2   SPEED

In considering system speed, it is necessary to differentiate between instantaneous and average speed. While the first may be impressive, it is the latter that is most important. Interruptions in system operation can produce an average throughput rate considerably lower than the maximum instantaneous rate.

For all practical purposes, the only moving parts in the COMAP system are the scanning beam galvanometers. It is conservative to say that the scanning beam can be brought to any given point within 10 msec. Assuming that the parallax data is required on a .333 mm x 0.333 mm grid (i.e. 10 points/mm^2), the scanner is able to cover 100 mm^2/sec. Since practical galvanometer scanners can run several times this speed, scanning beam positioning time is adequate for very fast operation (over 100 mm^2/sec).

79

Location of the correlation peak represents a more significant limit on system operation. If a conventional TV image tube is employed, a sampling rate of approximately 30 frames per second must be used. Assuming again that ten samples per mm^2 are required, the system coverage would be 3 mm^2/sec; a good, but not outstanding rate. This example makes it clear that correlation peak position measurement is one of the major factors limiting overall system speed.

Fortunately we are not limited to conventional TV image tubes for locating correlation peaks; there are, in fact, several alternative devices. These include solid state sensors (CCD's, CID's) and the image dissector. Solid state detectors offer a number of advantages; they are compact, rugged and metrically accurate. Moreover, they are not subject to the image retention (lag) characteristic of a vidicon and they may be scanned at a higher rate than 30 frames/sec.

Rapid and significant advances have been made in one and two dimensional solid state arrays. They are presently available with a sufficient number of resolution elements to serve as a correlation peak position measuring device. It seems probable that such a device could be made to operate at one hundred frames or more per second using present technology. This would imply an area coverage of at least 10 mm^2/sec in the COMAP system. A somewhat more sophisticated approach could yield sample rates several times as great as this.

The image dissector is interesting in that it offers the possibility of directly tracking the correlation peak as the scanning beam moves about the input gate. The dissector could operate in a star tracking mode or provide a small moving raster scan. This would limit the number of resolution elements sampled and could allow very rapid location of the correlation peak. Moreover, the dissector scan could be easily expanded to recapture the correlation peak when the scanning beam passes through regions of the

input which do not correlate. This would help to maintain a high average throughput rate. Control and calibration of an image dissector could be somewhat complicated but its potential flexibility recommends it for further consideration. The comparitively low sensitivity of an image detector might require undesirably high illumination levels at the input gate.

A significant feature of a COMAP system is its ability to automatically find the desired correlation after it has been lost for some reason. This can happen if the scanning beam illuminates a lake, snowfield, or other region which contains no useful detail. When such a situation arises, the scanning beam can simply be moved until a clearly identifiable correlation peak occurs in the output. Fill-in between regions of good correlation can be rapidly executed by extrapolating the probable path of the correlation peak and restricting peak detection to this area. This can be accomplished with any of the sensors discussed above by suitable video signal processing. Similarly abrupt changes in parallax can be handled readily since there is no need for maintaining an image-to-image lock in the COMAP system.

This self-finding ability should allow a COMAP system to maintain a high average as well as instantaneous throughput. Human intervention should not be required to help the system when regions of poor correlation or abrupt parallax shifts are encountered.

In summary, it should be relatively straightforward to design and build a COMAP-type system having an instantaneous throughput rate of about 10 mm^2/sec. A more sophisticated approach to the correlation peak detection problem could increase this throughput by an order of magnitude to 100 mm^2/sec. The average throughput rate of the system should be close to the instantaneous rate since the system can be made self-finding and human intervention can be minimized or eliminated.

Another important factor affecting the overall system speed is discussed under Data Format (Section 8. 3).

8.3   DATA FORMAT

A COMAP system allows extremely flexible data formatting in that the scanning beam may be directed to any point in the input. Scanning can be programmed to obtain data at arbitrary points in either photo or model coordinates. It is not necessary to collect data at one array of x, y coordinates and then convert this, by means of interpolation, to another array of coordinates (e. g. , from epipolar lines to a regular array in model coordinates). This can substantially reduce subsequent data processing and effectively increase the throughput rate of the overall system.

8.4   SIZE AND MOBILITY

The size of a COMAP system depends upon the frame size of the imagery. Folding the optics by means of mirrors can produce a very compact optical processor occupying say fifty cubic feet or less. The electronics involved could be fit into one or two standard racks. It is usually assumed that an automatic stereo compilation system such as this would be operated in a headquarters or laboratory environment. However, a COMAP system could be ruggedized and compacted to a tactical field support unit if desired. Where smaller frame size, say 70 mm or 5 inch imagery is involved, a very compact unit could be designed.

One problem with a non-laboratory environment is associated with spatial filters. This normally requires great system stability. However, by means of either short exposures using a pulsed laser or dynamic fringe (phase) control, stability requirements can be greatly relaxed and should represent no major difficulty.

8.5   OPERATIONAL CONVENIENCE

Most of the operations involved in a COMAP system can be made automatic. This includes, in particular, the filter making operation;

exposure and K ratio can be placed entirely under computer control. When measuring parallax, the operator may have to establish initially the interior orientation of an input and to specify control points. Data collection can then proceed automatically and operator intervention should not be required. The system can be designed to operate on roll film and there will be no need to separate and insert individual frames.

8.6   PANORAMIC IMAGERY

The COMAP system has only been demonstrated on vertical frame photography. Of course, panoramic and convergent panoramic imagery is of great interest. In order to handle panoramic photographs, it may be necessary to introduce anamorphic optics in the COMAP system. However, this has not been established as a firm requirement, and it is possible that such a complication may not be needed in cases of practical interest. This problem must yet be evaluated empirically.

8.7   OMNIDIRECTIONAL AIR BASE, SCALE AND ORIENTATION

Air base direction has no practical effect on COMAP system performance. The input transparency remains centered in the optical system regardless of the air base direction. The input must be oriented properly, but this is easily accomplished and could even be done automatically by measuring the intensity of the correlation peak produced by several local areas as the input is rotated. Depending upon the actual construction of the input gate assembly, any relative orientation between frames can be handled.

The system can also be arranged to handle limited variations in scale (say ±10%). This allows stereocompilation using side lapping as well as front lapping imagery and tolerates reasonable variations in altitude.

83

APPENDIX A

PARALLAX SCALE IN A COHERENT OPTICAL PROCESSOR

APPENDIX A

PARALLAX SCALE IN A COHERENT OPTICAL PROCESSOR

In a coherent optical processor employing a matched spatial filter, the location of a correlation peak is directly related to the position of the input signal. That is, if a signal $f(\bar{x})$ is located at position $\bar{x}_0$ when a filter is made and at $\bar{x}_1$ during the correlation operation, the resulting correlation peak will be located at a position $\bar{u}$ determined by $\bar{x}_1$ and $\bar{x}_0$. A simple analysis based on the correlation analogy implies $\bar{u} = \bar{x}_1 - \bar{x}_0$. However, the following analysis which considers the grating-like character of the hologram, indicates a more complex relation between $\bar{u}$ and $\bar{x}_1$, $\bar{x}_0$, i.e.,

$$u = \begin{bmatrix} a \\ b \end{bmatrix} [\bar{x} - \bar{x}_0]$$
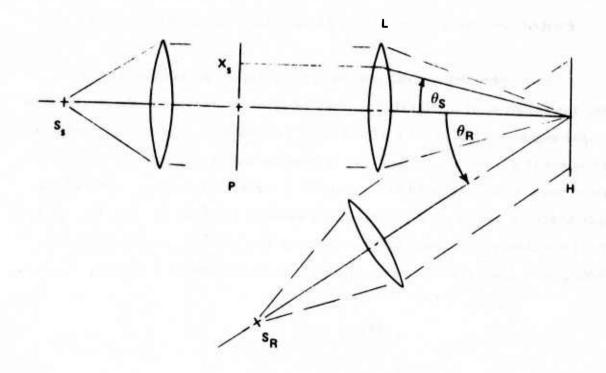
where $a \neq b$.

Consider the situation in Figure A-1 where a hologram is recorded in plane H. The correlations are formed by lens L_1 in the plane Q and $\bar{x}$ is a general point in the input plane P. During the correlation process, the reference source S_R is blocked.
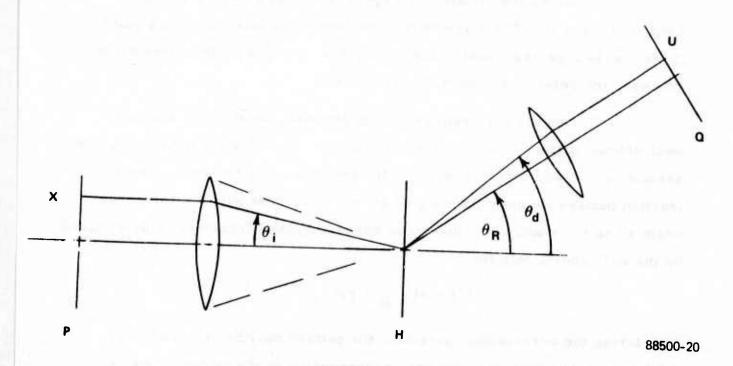
During the hologram recording process, let there be a small, well-defined pattern $f(\bar{x})$ centered at the point $\bar{x}_s$. For the time being, we assume $y = 0$ and that this is a two dimensional (x, z) problem. The diffraction pattern caused by the signal at $\bar{x}_s$ interferes with the reference beam so as to create a grating whose average spatial frequency is determined by the well-known relation

$$\lambda/d = \sin \theta_R + \sin \theta_S.$$

Now during the correlation operation, the pattern may be centered at any arbitrary x in which case the ray corresponding to the center of the pattern strikes the hologram at an angle

85

a. FILTER CONSTRUCTION

b. CORRELATION

88500-20

FIGURE A-1. PARALLAX SCALE DEFINITION

86

$$\theta_i = \arctan(x/F).$$

Without any loss of generality, we may set all focal lengths equal to unity so that x and u become normalized coordinates. This ray will be diffracted at an angle θ_d where

$$\sin \theta_i + \sin \theta_d = \lambda/d \cdot \sin \theta_R + \sin \theta_S.$$

The hologram will reconstruct the collimated reference beam at the angle θ_d. This reconstructed beam focuses to a correlation peak located at

$$u = \tan(\theta_d - \theta_R).$$

We are interested in determining u as a function of x_s and x_r the original and final locations of the pattern in question. In particular, we wish to determine the scale of the motion of the correlation peak relative to that of the input pattern. We need

$$M = \frac{du}{dx}$$

Now

$$u \quad \tan(\theta_d - \theta_R)$$

$$\theta_d \quad \arcsin(\sin \theta_R + \sin \theta_S - \sin \theta_i)$$

$$\theta_i = \arctan(x)$$

and

$$\frac{du}{dx} = \left(\frac{\partial u}{\partial \theta_d}\right)\left(\frac{\partial \theta_d}{\partial \theta_i}\right)\left(\frac{\partial \theta_i}{\partial x}\right)$$

$$\frac{\partial u}{\partial \theta_d} = \sec^2(\theta_d - \theta_R)$$

$$\frac{\delta \theta d}{\delta \theta_i} = [1 - (\sin \theta_R + \sin \theta_S - \sin \theta_i)^2]^{-\frac{1}{2}}$$

$$\frac{\delta \theta i}{\delta x} = (1 + x^2)^{-1}$$

If we assume the pattern moves only a small amount then we can evaluate these functions at $x = x_s$, $\theta_i = \theta_s$, $\theta_d = \theta_R$ so that

$$\frac{\delta u}{\delta \theta_d} = \sec^2 (0) = 1$$

$$\frac{\delta \theta d}{\delta \theta i} = [1 - \sin^2 \theta_R]^{-\frac{1}{2}} = \sec \theta_R$$

and

$$\frac{\delta \theta i}{\delta x} = [1 + x^2]^{-1}$$

$$M_x = \frac{du}{dx} = \frac{\sec \theta_R}{1 + x^2}$$

for small motions.

There is no grating effect in the orthogonal dimension so that

$$M_y = \frac{du}{dy} = 1$$

Of course, the results are normalized to the focal lengths of the transform and imaging lenses.

Actual measurements on the COMAP system using linear potentiometers gave,

$$M_x = \frac{1}{12.354} \text{ (arbitrary units)}$$

88

$$M_y = \frac{1}{15.767}$$

and

$$\frac{M_y}{M_x} = 0.7835$$

$$= \arccos (38.42)$$

A relatively crude direct measurement of θ_R indicates that $\theta_R = 38.5^o \ (\pm 0.25^o)$.

CONCLUSION

Parallax scale is a function of input position and reference beam angle. For a limited field and small parallax displacement, the parallax scales are

$$M_x \cong \sec (\theta_R)$$

$$M_y = 1.$$

When large fields and/or parallaxes are involved, a more sophisticated (and non-linear) relation must be used. In particular, the $(1 + x^2)^{-1}$ factor cannot be ignored.

APPENDIX B

HARTMAN MASK TEST

APPENDIX B

HARTMAN MASK TEST
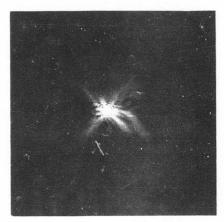
Insertion of a Hartman mask in the COMAP system signal beam revealed the presence of significant spherical aberration. The severity of this aberration makes it desirable to define the plane of non-paraxial focus as the filter plane. If the plane of paraxial focus is used, the intersection of the scanning beam with the filter plane is not constant, but depends upon the position of the scanning beam in the input plane. This makes final alignment of the scanner very difficult. If the non-paraxial plane of focus is chosen as the filter plane, the scanning beam remains stationary in the filter plane for all practical purposes.

We have not determined the exact cause of this spherical aberration. It could be introduced by the collimator or the large Fourier transform lens or both. While the aberration must be considered for alignment purposes, it has no significant effect on the basic correlation operation.
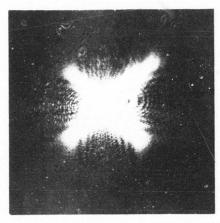
Figures B-1 and B-2 illustrate the effect of the spherical aberration in the signal beam. Figures B-1a and B-1b show the light intensity in the plane of paraxial focus. A short exposure (B-1a) reveals the usual Airy disc with some diagonal flare evident. A longer exposure (B-1b) shows the extent of this flare. The shape of the flare is caused by the 4" x 5" rectangular opening in the input gate.

Placing a mask in the input with two small (1 mm) off-axis, diametrically opposed holes produces the pattern of Figure B-1c in the paraxial focus plane. It is clear the non-paraxial rays do not intersect the center of the paraxial plane.
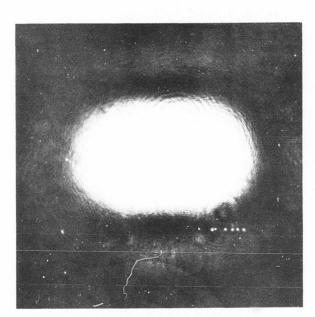
Figures B-2a, b and c show the corresponding situation in the plane of non-paraxial focus. This plane is 750μm from the paraxial focus.
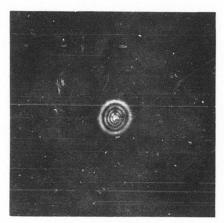
(a) FULL APERTURE FOCUS
(PLANE OF PARAXIAL FOCUS)

(b) FULL APERTURE FOCUS (OVEREXPOSED)
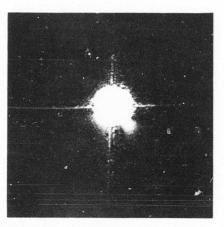(PLANE OF PARAXIAL FOCUS)

(c) FOCUS OF HARTMANN MASK
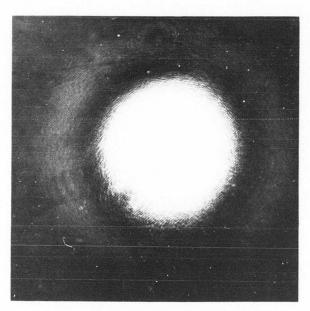(PLANE OF PARAXIAL FOCUS)

FIGURE B-1.   SIGNAL BEAM HARTMANN TEST,
PLANE OF PARAXIAL FOCUS

(a)   FULL APERTURE FOCUS
(PLANE OF NONPARAXIAL FOCUS)

(b)   FULL APERTURE FOCUS (OVEREXPOSED)
(PLANE OF NONPARAXIAL FOCUS)

(c)   FOCUS OF HARTMANN MASK
(PLANE OF NONPARAXIAL FOCUS)

FIGURE B-2.   SIGNAL BEAM HARTMANN TEST,
PLANE OF NON-PARAXIAL FOCUS

MISSION
of
Rome Air Development Center

*RADC is the principal AFSC organization charged with
planning and executing the USAF exploratory and advanced
development programs for information sciences, intelli-
gence, command, control and communications technology,
products and services oriented to the needs of the USAF.
Primary RADC mission areas are communications, electro-
magnetic guidance and control, surveillance of ground
and aerospace objects, intelligence data collection and
handling, information system technology, and electronic
reliability, maintainability and compatibility. RADC
has mission responsibility as assigned by AFSC for de-
monstration and acquisition of selected subsystems and
systems in the intelligence, mapping, charting, command,
control and communications areas.*